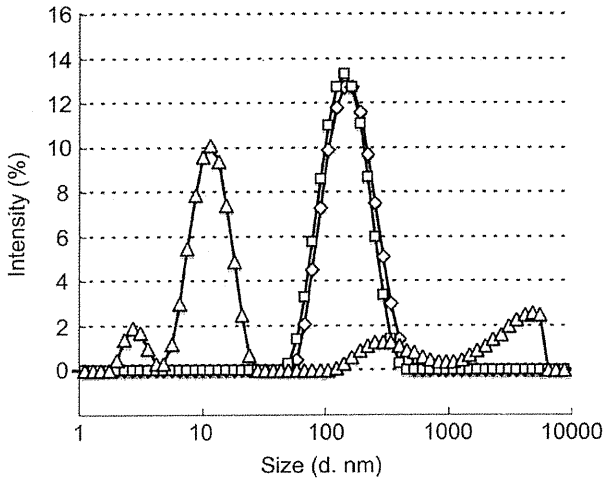

Fig. 3. Size distribution of PICs prepared from the polyaspartamide derivatives at *N/P* = 10 in 10 mM HEPES buffer (pH 7.4) (siRNA: 4 μM). Each symbol represents PAsp(TEP) PIC (open diamond), PAsp(DPT) PIC (open square), and PAsp(DET) PIC (open triangle).

PAsp(DET) had a polydispersed size distribution with a substantially smaller size (~10 nm) as a major fraction in the same buffer. Note that the presence of the small PICs in PAsp(DET) was also observed in the following fluorescence correlation spectroscopy (FCS) analysis (Fig. 4A). These results suggest that higher charge density and the number of protonated amino groups in the side chain may facilitate the formation of PIC particles with narrow size distribution, presumably through the enhanced multivalent interaction with siRNA molecules.

The FCS analysis, which enables the size estimate of fluorescently labeled molecules even in serum-containing media [21,22,28], was conducted to investigate the PIC stability in the cell culture medium containing 10% FBS. Based on the Stokes–Einstein equation with the assumption that PICs prepared were spherical structures, the diffusion coefficients of siRNA-loaded PICs obtained by FCS analysis were converted to the corresponding hydrodynamic radius to obtain the diameter of PICs. siRNA/PAsp(DET) PIC decreased its size to the similar level of naked siRNA molecules (Fig. 4A) within 5 min after the serum addition, indicating the prompt dissociation of the PIC to release free siRNA in the serum-containing medium. In contrast, siRNA/PAsp(TEP) and siRNA/PAsp(DPT) PICs showed no decrease in the size even after 1 h incubation in the serum-containing medium (Fig. 4B), indicating that their PICs were more tolerable in the serum-containing medium. The sizes of these PICs were increased immediately in the serum-containing medium, suggesting the interaction with serum components, most likely anionic serum proteins thereby forming secondary aggregates. The higher charge density and number in the side chain of PAsp(TEP) and PAsp(DPT) are more likely to facilitate a local multivalent binding of the repeating array of positively charged amino groups in the polymer to siRNA phosphates, rendering the PIC tolerable against an exchange with anionic serum proteins.

3.3. Gene silencing study

Gene silencing efficiency of the siRNA-loaded PICs from the cationic polyaspartamide derivatives was examined using B16F10-Luc, a mouse melanoma cell line stably expressing luciferase, by measuring the luciferase luminescence intensity in the cells treated by each PIC after incubation for 48 h (Fig. 5). The significant gene

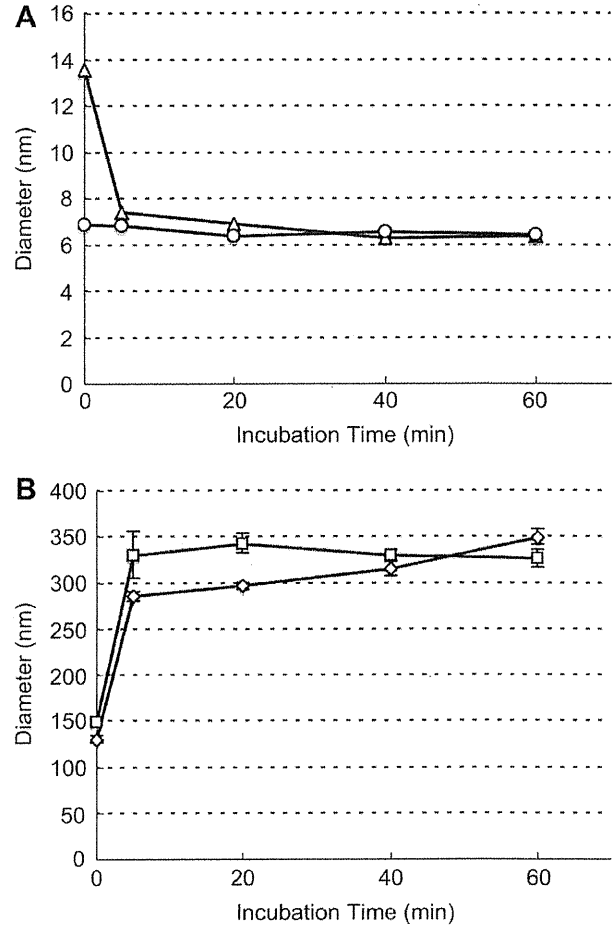

Fig. 4. Time-dependent change in the diameter of (A) PAsp(DET) PIC (open triangle) and naked siRNA (open circle), (B) PAsp(TEP) PIC (open diamond) and PAsp(DPT) PIC (open square) in the cell culture medium (10% FBS). PICs were prepared at *N/P* = 10, and siRNA concentration was set to 100 nM. The diameters were calculated from the diffusion coefficients measured by fluorescence correlation spectroscopy analysis. Results are expressed as the mean ± S.D. (*n* = 10).

silencing was observed in siRNA/PAsp(TEP) PIC at *N/P* = 10 and 20, siRNA/PAsp(DPT) PIC at *N/P* = 10, and ExGen 500 (a linear PEI-based transfection reagent as a control) at *N/P* = 10 and 20, whereas no significant gene silencing was observed for the cells treated by siRNA/PAsp(DET) PIC at *N/P* = 10 and 20. These results were well correlated with the serum tolerability of these PICs. The PICs from PAsp(TEP) and PAsp(DPT) showing high stability in the serum-containing media (Fig. 4) exerted significant gene silencing. Meanwhile, the PAsp(TEP) PICs loaded with scrambled siRNA induced no reduction in the luciferase expression, thus it was confirmed that the decrease in the luciferase expression by PAsp(TEP) PICs with luciferase siRNA was indeed caused by the sequence-dependent gene silencing of siRNA. In contrast, PAsp(DPT) and ExGen 500 PICs with scrambled siRNA resulted in the considerable reduction of luciferase gene expression, especially at *N/P* = 20, due to the severe cytotoxicity of these PICs regardless of siRNA sequence. In fact, a colorimetric cell viability assay revealed the strong cytotoxicity of PAsp(DPT) and ExGen 500 PICs at the higher *N/P* ratio (Fig. 6). Alternatively, PAsp(TEP) induced almost no decrease in the cell viability in this transfection condition, achieving effective gene silencing with negligible cytotoxicity.

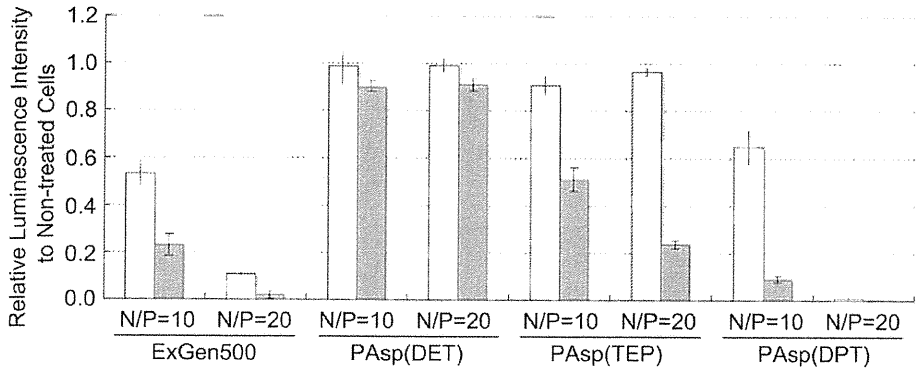

Fig. 5. Gene silencing efficiency of PICs evaluated by luciferase assay with B16F10-Luc cells. Scrambled siRNA (white bar) was adopted as a control sequence for luciferase siRNA (gray bar). Luciferase expression was measured after 48 h incubation with the PICs (siRNA: 100 nM). Results are expressed as the mean ± S.D. ($n = 4$).

3.4. Cellular uptake and intracellular distribution studies

To obtain an insight into the critical step in the transfection with the siRNA-loaded PICs tested here, the cellular uptake and intracellular distribution profiles were compared among the PICs. In the cellular uptake study, B16F10-Luc cells were treated by Cy3-siRNA-loaded PICs in the condition showing no severe cytotoxicity ($N/P = 10$ and 20 for PAsp(DET)/PAsp(TEP) and $N/P = 10$ for PAsp(DPT)) for 12 h, and then fluorescent signal from the cells was detected with a flow cytometer (Fig. 7). The cells treated by PAsp(TEP) and PAsp(DPT) PICs had one order of magnitude higher mean fluorescence intensity than those treated by PAsp(DET) PICs ($P < 0.01$), which showed the mean fluorescence comparable to the cells treated by naked Cy3-siRNA. This result indicated that the significant cellular uptake of PICs was achieved in the PAsp(DPT) and PAsp(TEP) system but not PAsp(DET) system. The obtained cellular uptake profiles were well correlated with the results of the stability (Fig. 4) and the gene silencing activity (Fig. 5) of the PICs, strongly suggesting that the stable PIC formation facilitated the cellular uptake of siRNA to exert effective gene silencing against the cultured cells. Interestingly, despite the similar PIC stability in the cell culture medium (Fig. 4), more efficient cellular uptake was observed for PAsp(DPT) PICs compared to PAsp(TEP) PICs ($P < 0.01$). The higher charge density in the side chain of PAsp(DPT) at pH 7.4 might facilitate the interaction of the PICs with the anionic components of cytoplasmic membrane leading to an increased efficiency of endocytosis [29]. Nevertheless, strong affinity of PAsp(DPT) with cytoplasmic membranes might impede the membrane integrity even at pH 7.4, causing a substantial increase in the cytotoxicity as seen in Fig. 6 [14].

Another critical step in siRNA delivery into the cytoplasm is endosomal escape [30]. The confocal laser scanning microscopic (CLSM) observation was performed to investigate the intracellular trafficking of Cy3-siRNA/PAsp(TEP) PIC at $N/P = 20$ and Cy3-siRNA/PAsp(DPT) PIC at $N/P = 10$, which achieved effective gene silencing without severe cytotoxicity (Figs. 5 and 6), by staining late endosome/lysosome and nucleus with LysoTracker Green (green) and Hoechst33342 (blue), respectively. Thus, in the CLSM images, the colocalization of Cy3-siRNA (red) with late endosome/lysosome (green) should be detected as yellow pixels. Fig. 8 clearly displayed the fluorescent signal from Cy3-siRNA (red and yellow pixels) within the cells treated by PAsp(TEP) and PAsp(DPT) PICs, consistent with the effective siRNA uptake as seen in the flow cytometric analysis (Fig. 7). To quantitatively estimate the endosomal escape of each PIC, the colocalization ratio of Cy3-siRNA with late endosome/lysosomes was determined from the ratio of the number of yellow pixels to the number of yellow/red pixels [22]. The colocalization ratios of Cy3-siRNA delivered by PICs were calculated to be ~26%

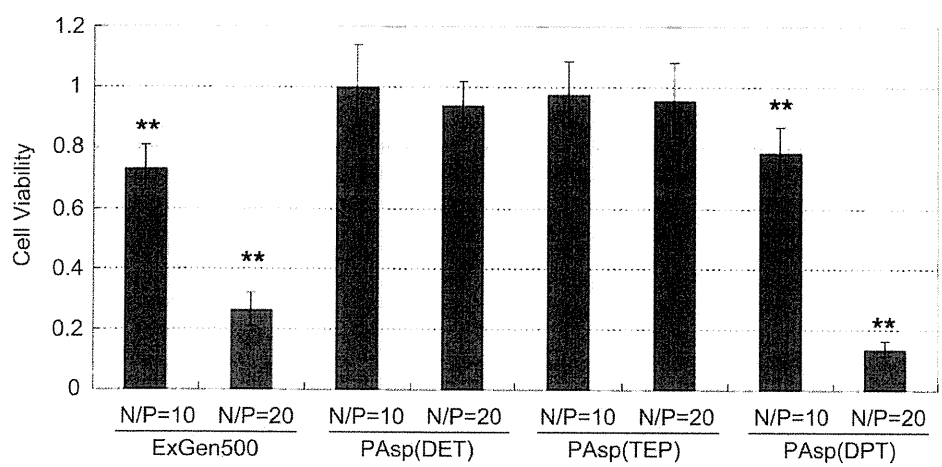

Fig. 6. Cytotoxicity of siRNA PICs against B16F10-Luc cells (siRNA: 100 nM) under the same condition as in the luciferase assay. Results are expressed as the mean ± S.D. ($n = 8$). ** indicates that the cells treated with each polyaspartamide derivative showed a significantly lower cell viability compared to the cells without any treatment ($P < 0.01$).

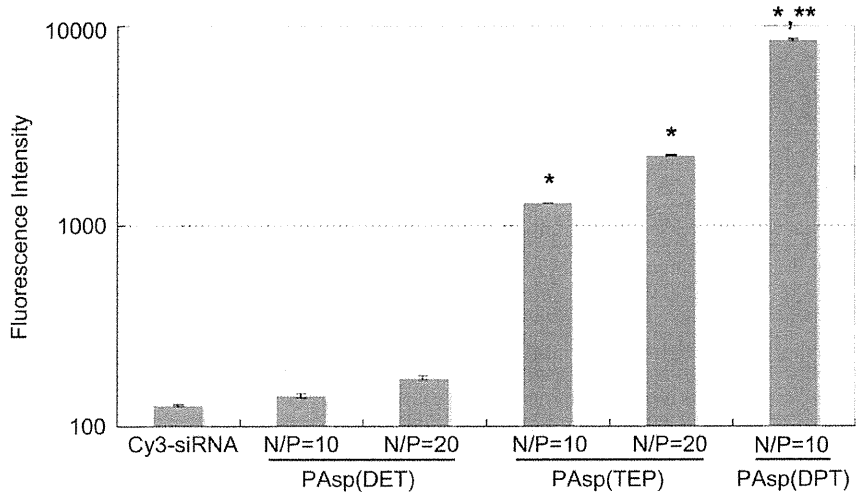

Fig. 7. Cellular uptake of siRNA PICs (siRNA: 100 nM) by B16F10-Luc cells after 12 h incubation measured with a flow cytometer. Results are expressed as the mean ± S.D. ($n = 3$). * indicates that cellular uptake of PICs was significantly higher than PAsp(DET) PIC and naked siRNA ($P < 0.01$). ** indicates that cellular uptake of PICs was significantly higher than PAsp(TEP) PICs prepared at N/P = 10 and 20 ($P < 0.01$).

for PAsp(TEP) at $N/P = 20$ and ~20% for PAsp(DPT) at $N/P = 10$, indicating that major portions of intracellular Cy3-siRNAs (~74% for PAsp(TEP) at $N/P = 20$ and ~80% for PAsp(DPT) at $N/P = 10$) were not distributed in late endosomal/lysosomal compartments 24 h after PIC administration, probably due to efficient endosomal escape. Note that the fluorescent signal of Cy3-siRNA from the cells treated by naked Cy3-siRNA or PAsp(DET) PICs was scarcely detected in this experimental condition (data not shown), corresponding to the poor siRNA uptake as seen in Fig. 7. Thus, we concluded that PAsp(TEP) and PAsp(DPT) appreciably improved both cellular uptake and endosomal escape of siRNA-loaded into their PICs.

3.5. Cellular membrane destabilization activity

From the results obtained in the preceding sections, PAsp(TEP) and PAsp(DPT) PICs were confirmed to facilitate cellular uptake and endosomal escape of loaded siRNA (Figs. 7 and 8), and consequently achieved the significant gene silencing (Fig. 5). However, the gene silencing of PAsp(DPT) PICs was accompanied by the cytotoxicity, which was in sharp contrast to PAsp(TEP) PICs showing comparable gene silencing without marked cytotoxicity (Fig. 6). Cytotoxicity of polycations is explained by the induction of impaired integrity of cytoplasmic membranes through their direct interaction with the anionic components of cytoplasmic membranes [11,14]; this mechanism may also play a role in an escape of polycation-based siRNA carriers from the acidic endosomal compartment. It should be noted that smart polycations increasing the capability to destabilize the membrane selectively in acidic milieu of endosome may lead to efficient but less toxic endosomal escape of their PICs [14].

Based on the fact that the side chain of PAsp(TEP) changed from the di-protonated state at pH 7.4 to tri-protonated state at pH 5.5 (Fig. 2), PAsp(TEP) is expected to have the acidic pH-selective membrane destabilization similar to PAsp(DET). We therefore evaluated the induction of the membrane destabilization by PAsp(TEP) in comparison with PAsp(DPT) and PAsp(DET) against B16F10-Luc cells at both extracellular pH of 7.4 and endosomal pH of 5.5. This study was evaluated by measuring the increased membrane permeability of YO-PRO-1 dye after incubating the cells with the polycations for 20 min (Fig. 9 and Fig. S1) [26]. Note that YO-PRO-1 is a cyanine dye staining DNA in the nucleus but it cannot permeate an intact cytoplasmic membrane of living cells. Therefore, the increased fluorescent signals of permeated YO-PRO-1 from living cell nuclei are expected to reflect the degree of membrane destabilization that would be induced by the polycations. As shown in Fig. 9, the cells treated with PAsp(TEP) exhibited negligible YO-PRO-1 fluorescence intensity at pH 7.4, while at pH 5.5 the PAsp(TEP) treatment induced a significant increase in the YO-PRO-1 fluorescence, indicating that PAsp(TEP) held the acidic pH-selective membrane destabilization capability in a similar manner as PAsp(DET). In contrast, PAsp(DPT) induced a significant increase in the YO-PRO-1 fluorescence corresponding to the strong membrane destabilization effect at both pH 7.4 and 5.5, which is consistent with its high cytotoxicity even under the physiological condition (Fig. 6).

In order to gain the insight into the mechanism of the membrane destabilization effect shown in Fig. 9, we focused on the types of polycations and their protonated structure varying with environmental pH. The significant increase in the YO-PRO-1 fluorescence compared to control was observed for PAsp(TEP) at pH 5.5, PAsp(DET) at pH 5.5, and PAsp(DPT) at pH 7.4 and 5.5 ($P < 0.01$), indicating the impaired membrane integrity In particular, the strongest effect was induced by PAsp(TEP) at pH 5.5. These trends suggest that the membrane destabilization effects might have some correlation with the number of protonated amines in the side chain of the polycations. Nevertheless, PAsp(TEP) at pH 7.4 displayed no significant membrane destabilization effect despite the side chain containing two protonated amines as PAsp(DPT). Of note is the spacer between two protonated amines in the side chain of each polycation (Fig. 2). The strong membrane destabilization was observed for the polycations with side chains having two protonated amines separated by the shorter spacers, i.e., ethylene spacer ($-CH_2CH_2-$) in PAsp(DET) and PAsp(TEP) at pH 5.5 and propylene spacer ($-CH_2CH_2CH_2-$) in PAsp(DPT) at pH 7.4 and 5.5. Alternatively, two protonated amines are separated by the longer spacer ($-CH_2CH_2NHCH_2CH_2-$ or $-CH_2CH_2NHCH_2CH_2NHCH_2CH_2-$) in PAsp(TEP) at pH 7.4. These results indicate that not only the number of cationic charges in the side chain but also their spacer length between protonated amines should be crucial to induce the membrane destabilization. The repeated protonated amines with shorter spacer length might enhance the capacity to perturb the

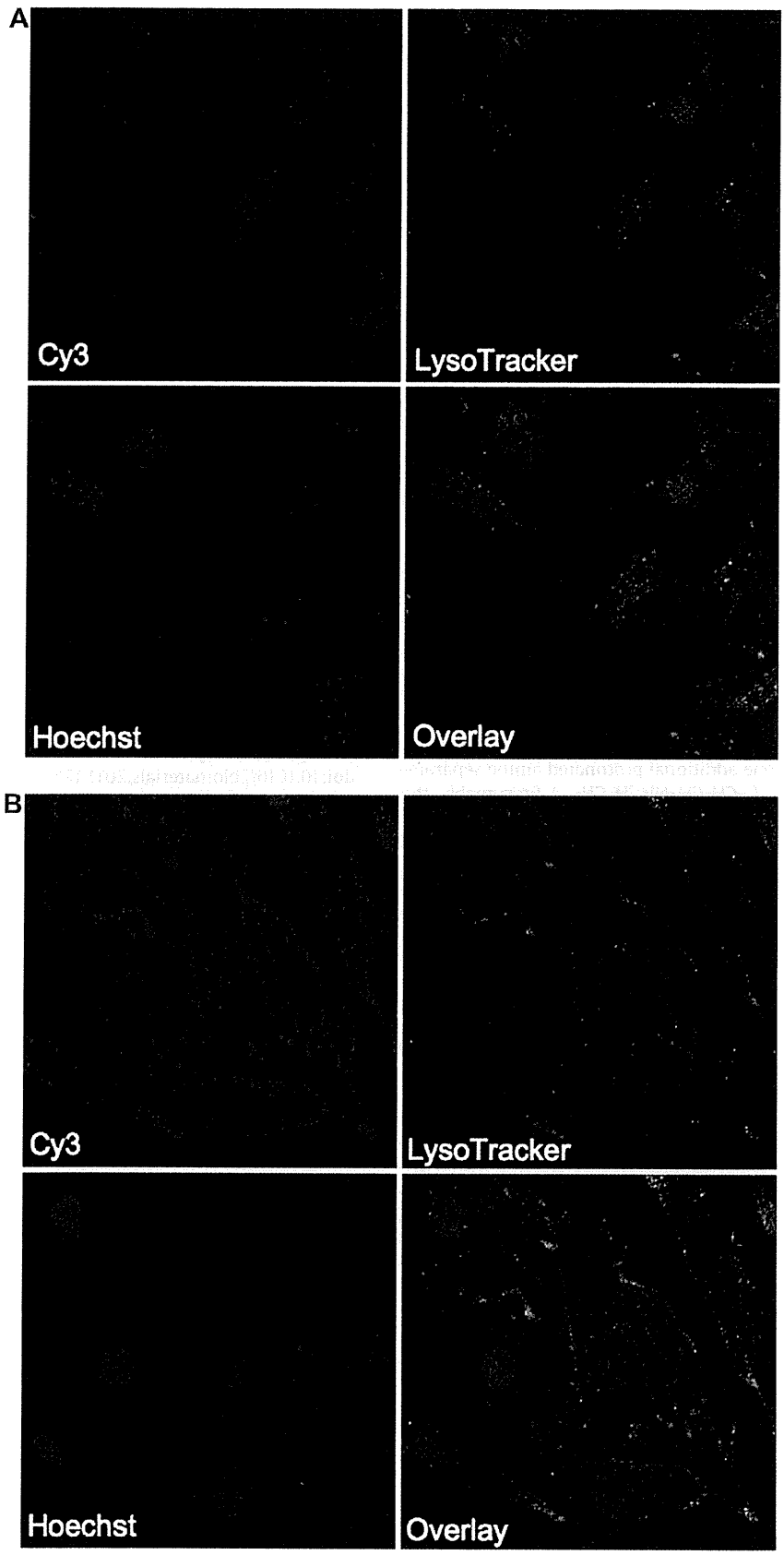

Fig. 8. Intracellular distribution of Cy3-siRNA PICs (siRNA: 100 nM) in B16F10-Luc cells after 24 h incubation, observed with confocal laser scanning microscope (Red: Cy3-siRNA, Green: LysoTracker Green, Blue: Hoechst33342). Each image represents the cells treated by PAsp(TEP) at $N/P = 20$ (A) and PAsp(DPT) at $N/P = 10$ (B). (For interpretation of the references to colour in this figure legend, the reader is referred to the web version of this article.)

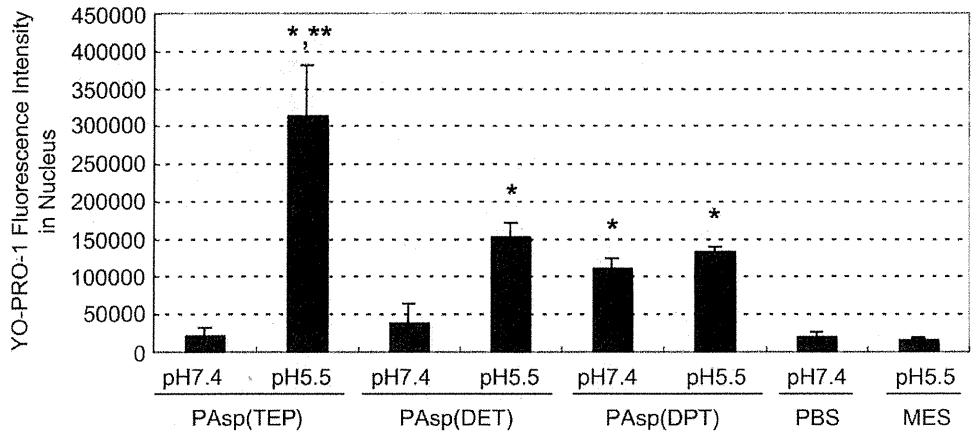

Fig. 9. Cellular membrane destabilization activity of each polyaspartamide derivative evaluated from the membrane permeability of YO-PRO-1 after incubation for 20 min with polyaspartamide derivatives, measured with In Cell Analyzer. The concentration of polycations was corresponding to that of PICs prepared at $N/P = 10$ in the luciferase assay. Results are expressed as the mean ± S.D. ($n = 3$). * indicates that the cells treated with each polyaspartamide derivative showed a significantly higher YO-PRO-1 fluorescence than cells treated with control (PBS for the treatment at pH 7.4 and MES for the treatment at pH 5.5) ($P < 0.01$), ** indicates that cells treated with PAsp(TEP) at pH 5.5 showed a significantly higher YO-PRO-1 fluorescence than cells treated with other polyaspartamide derivatives at pH 7.4 ($P < 0.01$) and pH 5.5 ($P < 0.05$).

membrane integrity through the facilitated binding of a multivalent array of cationic charges to the anionic component of cytoplasmic membrane. In line with this mechanism, PAsp(TEP) exerted appreciably high membrane disturbance effects at lowered pH of 5.5, where it took a tri-protonated state as a major component with two protonated amines linked by an ethylene spacer, fixing into *anti* conformation, and one additional protonated amine separated by flexible longer spacer ($-CH_2CH_2NHCH_2CH_2-$). Presumably, this characteristic arrayed structure of positive charges in PAsp(TEP) may lead to the unique and significant pH selectivity in YO-PRO-1 permeation through cytoplasmic membrane as seen in Fig. 9, thereby leading to effective endosomal escape and subsequent gene silencing with minimal cytotoxicity of siRNA/PAsp(TEP) PIC as demonstrated in Figs. 5, 6 and 8.

4. Conclusion

High stability both in storage condition and in biological milieu after the administration, effective cellular uptake with low cytotoxicity, and efficient endosomal escape leading to target-specific gene silencing are the major prerequisites for PIC-based siRNA carriers. The formation of stable siRNA-loaded PICs was demonstrated here from cationic polyaspartamide derivatives with a pH-valuable repeated array of protonated amines, exerting multivalent binding to siRNA molecules. Consequently, the constructed PIC achieved efficient cellular uptake due to enough tolerability in serum-containing medium and pH-selective disruption of cytoplasmic membranes for endosomal escape with minimal cytotoxicity and subsequent gene silencing with high efficiency. The number and the spacing length of repeating amino groups in the side chain of the polycations play a key role in these unique characteristics of the PIC, and the fine-tuning of these parameters is indispensable for translating PIC-based siRNA carriers into practical settings.

Acknowledgments

This research is granted by the Japan Society for the Promotion of Science (JSPS) through the "Funding Program for World-Leading Innovative R&D on Science and Technology (FIRST Program)," initiated by the Council for Science and Technology Policy (CSTP).

We express our appreciation to Dr. Darin Y. Furgeson (University of Utah) for proofreading of this manuscript.

Appendix. Supplementary material

Supplementary data related to this article can be found online at doi:10.1016/j.biomaterials.2011.12.022.

References

[1] Whitehead KA, Langer R, Anderson DG. Knocking down barriers: advances in siRNA delivery. Nat Rev Drug Discov 2009;8:129–38.
[2] Kabanov AV, Kabanov VA. DNA complexes with polycations for the delivery of genetic material into cells. Bioconjug Chem 1995;6:7–20.
[3] Kakizawa Y, Kataoka K. Block copolymer micelles for delivery of gene and related compounds. Adv Drug Deliv Rev 2002;54:203–22.
[4] Nishiyama N, Kataoka K. Current state, achievements, and future prospects of polymeric micelles as nanocarriers for drug and gene delivery. Pharm Ther 2006;112:630–48.
[5] Frohlich T, Wagner E. Peptide- and polymer-based delivery of therapeutic RNA. Soft Matter 2010;6:226–34.
[6] Boussif O, Lezoualc'h F, Zanta MA, Mergny MD, Scherman D, Demeneix B, et al. A versatile vector for gene and oligonucleotide transfer into cells in culture and in vivo: polyethylenimine. Proc Natl Acad Sci USA 1995;92:7297–301.
[7] Neu M, Fischer D, Kissel T. Recent advances in rational gene transfer vector design based on poly(ethylene imine) and its derivatives. J Gene Med 2005;7:992–1009.
[8] Schiffelers RM, Ansari A, Xu J, Zhou Q, Tang Q, Storm G, et al. Cancer siRNA therapy by tumor selective delivery with ligand-targeted sterically stabilized nanoparticle. Nucleic Acids Res 2004;32:e149.
[9] Ge Q, Filip L, Bai A, Nguyen T, Eisen HN, Chen J. Inhibition of influenza virus productin in virus-infected mice by RNA interference. Proc Natl Acad Sci USA 2004;101:8676–81.
[10] Alshamsan A, Haddadi A, Incani V, Samuel J, Lavasanifar A, Uludag H. Formulation and delivery of siRNA by oleic acid and stearic acid modified polyethylenimine. Mol Pharmaceutics 2009;6:121–33.
[11] Fischer D, Li Y, Ahlemeyer B, Krieglstein J, Kissel T. In vitro cytotoxicity testing of polycations: influence of polymer structure on cell viability and hemolysis. Biomaterials 2003;24:1121–31.
[12] Moghimi SM, Symonds P, Murray JC, Hunter AC, Debska G, Szewczyk A. A two-stage poly(ethylenimine)-mediated cytotoxicity: implications for gene transfer/therapy. Mol Ther 2005;11:990–5.
[13] Hunter AC. Molecular hurdles in polyfectin design and mechanistic background to polycation induced cytotoxicity. Adv Drug Deliv Rev 2006;58:1523–31.
[14] Miyata K, Oba M, Nakanishi M, Fukushima S, Yamasaki Y, Koyama H, et al. Polyplexes from poly(aspartamide) bearing 1,2-diaminoethane side chains induce pH-selective, endosomal membrane destabilization with amplified transfection and negligible cytotoxicity. J Am Chem Soc 2008;130:16287–94.
[15] Kanayama N, Fukushima S, Nishiyama N, Itaka K, Jang WD, Miyata K, et al. A PEG-based biocompatible block catiomer with high buffering capacity for

the construction of polyplex micelles showing efficient gene transfer toward primary cells. ChemMedChem 2006;1:439–44.
[16] Masago K, Itaka K, Nishiyama N, Chung UI, Kataoka K. Gene delivery with biocompatible cationic polymer: pharmacogenomic analysis on cell bioactivity. Biomaterials 2007;28:5169–75.
[17] Akagi D, Oba M, Koyama H, Nishiyama N, Miyata T, Nagawa H, et al. Biocompatible micellar nanovectors achieve efficient gene transfer to vascular lesions without cytotoxicity and thrombus formation. J Gene Med 2008;10. pp. 474–474.
[18] Itaka K, Ohba S, Miyata K, Kawaguchi H, Nakamura K, Takato T, et al. Bone regeneration by regulated in vivo gene transfer using biocompatible polyplex nanomicelles. Mol Ther 2007;15:1655–62.
[19] Harada-Shiba M, Takamisawa I, Miyata K, Ishii T, Nishiyama N, Itaka K, et al. Intratracheal gene transfer of adrenomedullin using polyplex nanomicelles attenuates monocrotaline-induced pulmonary hypertension in rats. Mol Ther 2009;17:1180–6.
[20] Oba M, Miyata K, Osada K, Christie RJ, Sanjoh M, Li W, et al. Polyplex micelles prepared from ω-cholesteryl PEG-polycation block copolymers for systemic gene delivery. Biomaterials 2011;32:652–63.
[21] Kim HJ, Ishii A, Miyata K, Lee Y, Wu S, Oba M, et al. Introduction of stearoyl moieties into a biocompatible cationic polyaspartamide derivative, PAsp(-DET), with endosomal escaping function for enhanced siRNA-mediated gene knockdown. J Control Release 2010;145:141–8.
[22] Takemoto H, Ishii A, Miyata K, Nakanishi M, Oba M, Ishii T, et al. siRNA-grafted polymer for polyion complex (PIC)-based siRNA delivery: enhancement of PIC stability and gene silencing efficiency. Biomaterials 2010;31:8097–105.
[23] Itaka K, Ishii T, Hasegawa Y, Kataoka K. Biodegradable polyamino acid-based polycations as safe and effective gene carrier minimizing cumulative toxicity. Biomaterials 2010;31:3707–14.
[24] Uchida H, Miyata K, Oba M, Ishii T, Suma T, Itaka K, et al. Odd-even effect of repeating aminoethylene units in the side chain of *N*-substituted polyaspartamides on gene transfection profiles. J Am Chem Soc 2011;133:15524–32.
[25] Harada A, Kataoka K. Formation of polyion complex micelles in an aqueous milieu from a pair of oppositely-charged block copolymers with poly(ethylene glycol) segments. Macromolecules 1995;28:5294–9.
[26] Uchida S, Itaka K, Chen Q, Osada K, Miyata K, Ishii T, et al. Combination of chondroitin sulfate and polyplex micelles of poly(ethylene glycol)-poly{N'-[N-(2-aminoethyl)-2-aminoethyl]aspartamide} block copolymer for prolonged in vivo gene transfection with reduced toxicity. J Control Release 2011;155:296–302.
[27] Nakanishi M, Park J-S, Jang W-D, Oba M, Kataoka K. Study of the quantitative aminolysis reaction of poly(β-benzyl L-aspartate) (PBLA) as a platform polymer for functionality materials. React Funct Polym 2007;67:1361–72.
[28] Buyens K, Meyer M, Wagner E, Demeester J, De Smedt SC, Sanders NN. Monitoring the disassembly of siRNA polyplexes in serum is crucial for predicting their biological efficacy. J Control Release 2010;141:38–41.
[29] Mislick KA, Baldeschwieler JD. Evidence for the role of proteoglycans in cation-mediated gene transfer. Proc Natl Acad Sci USA 1996;93:12349–54.
[30] Khalil IA, Kogure K, Akita H, Harashima H. Uptake pathways and subsequent intracellular trafficking in nonviral gene delivery. Pharmacol Rev 2006;58:32–45.

Journal of Drug Targeting, 2011, 1–10, Early Online

ISSN 1061-186X print/ISSN 1029-2330 online
DOI: 10.3109/1061186X.2011.632010

informa
healthcare

RESEARCH ARTICLE

PEG-detachable cationic polyaspartamide derivatives bearing stearoyl moieties for systemic siRNA delivery toward subcutaneous BxPC3 pancreatic tumor

Hyun Jin Kim[1], Makoto Oba[2], Frederico Pittella[3], Takahiro Nomoto[3], Horacio Cabral[3], Yu Matsumoto[4], Kanjiro Miyata[4], Nobuhiro Nishiyama[4], Kazunori Kataoka[1,3,4,5]

[1]*Department of Materials Engineering, Graduate School of Engineering, The University of Tokyo, Tokyo, Japan,* [2]*Department of Clinical Vascular Regeneration, Graduate School of Medicine, The University of Tokyo, Tokyo, Japan,* [3]*Department of Bioengineering, Graduate School of Engineering, The University of Tokyo, Tokyo, Japan, and* [4]*Center for Disease Biology and Integrative Medicine, Graduate School of Medicine, The University of Tokyo, Tokyo, Japan, and* [5]*Center for NanoBio Integration, The University of Tokyo, Tokyo, Japan*

Abstract

For systemic siRNA delivery into tumor tissues, a safe and efficient vehicle is strongly required. Therefore, we designed a block copolymer of detachable poly(ethylene glycol) (PEG) polycation bearing low pKa amines and hydrophobic moieties in the side chain to develop a smart siRNA complex possessing biocompatibility, high complex stability, and endosomal escaping functionality. A disulfide linkage (-SS-) was inserted as a linker between PEG and a cationic polyaspartamide derivative, poly{*N*-[*N*-(2-aminoethyl)-2-aminoethyl]aspartamide} (PAsp(DET)), with a flanking stearoyl moiety, where PAsp(DET) segment provides the excellent ability of endosome destabilization by direct interaction with the membrane. The resulting polymer, stearoyl PEG-SS-PAsp(DET), was confirmed to form the siRNA complex with an environment-responsive PEG palisade, which was detached from the complex surface under reductive conditions mimicking tumor tissues and cytoplasm because of the disulfide cleavage. The smart siRNA complex allowed significant gene silencing against cultured pancreatic cancer cells without considerable cytotoxicity and erythrocyte disruption, whereas such significant gene silencing was not observed in a control siRNA complex without the disulfide linkage. This enhanced gene silencing activity might be because of the enhanced cellular uptake and subsequent translocation of siRNA into cytoplasm facilitated by PEG detachment around and/or in the cancer cells. Further, intravital real-time confocal laser scanning microscopic observation revealed the effect of hydrophobic stearoyl modification on the stabilization of the siRNA complex for longevity in the blood. Significant *in vivo* gene silencing of the smart siRNA complex was achieved by systemic administration of vascular endothelial growth factor siRNA in a mouse model bearing a subcutaneous pancreatic tumor, leading to 40% regression in tumor growth. These results demonstrate the strong potential of stearoyl PEG-SS-PAsp(DET) as a vehicle for systemic delivery of siRNA in cancer therapy.

Keywords: siRNA delivery, antiangiogenesis, stearoylation, polyaspartamide

Introduction

Recently, RNA interference (RNAi) technology, in which small interfering RNA (siRNA) induces the degradation of messenger RNA (mRNA) of the target gene, has been widely developed for therapeutic applications. Cancer is one of the major target diseases for siRNA therapies (Aagaard & Rossi, 2007), because silencing of several target genes, such as oncogenes, by siRNA has been reported to successfully induce cancer cells apoptosis under culture conditions (Dykxhoorn, 2009, He et al., 2009). For clinical anticancer therapy, systemic administration of siRNA is essential to access a broad range of tumor tissues. However, in the systemic route, siRNA encounters substantial barriers before reaching the target tumor cytoplasm, such as nuclease attack, renal clearance, nonspecific interaction with blood components, cytoplasmic

Address for Correspondence: Kazunori Kataoka, Department of Materials Engineering, Graduate School of Engineering, The University of Tokyo, 7-3-1 Hongo, Bunkyo-ku, Tokyo 113-8656, Japan. Tel: +81 3 5841 7138. Fax: +81 3 5841 7139. E-mail: kataoka@bmw.t.u-tokyo.ac.jp

(Received 09 July 2011; revised 15 September 2011; accepted 18 September 2011)

membrane, and endosomal entrapment in tumor cells (Christie et al., 2010). The primary prerequisite to allow *in vivo* RNAi is high complex stability between siRNA and delivery carrier enough to tolerate under harsh *in vivo* conditions. The longevity of siRNA complexes in the bloodstream should lead to their increased accumulation in tumor tissues through leaky blood vasculature, which is called enhanced permeability and retention (EPR) effect (Fang et al., 2011). Delivery carriers of siRNA have been extensively developed to overcome these barriers by investigating cationic lipids and polycations (Whitehead et al., 2009), which allow the formation of a polyion complex with siRNA that protects against the enzymatic degradation and facilitates cellular uptake. Nevertheless, successful *in vivo* siRNA carriers have not yet been established, although several clinical trials are currently underway (Whitehead et al., 2009).

In a previous study, we developed a cationic polyaspartamide derivative bearing hydrophobic moieties in the side chain to prepare a siRNA complex with high complex stability and endosomal escaping functionality (Kim et al., 2010). Indeed, poly{*N*-[N-(2-aminoethyl)-2-aminoethyl]aspartamide} (PAsp(DET)) was synthesized by aminolysis of poly(β-benzyl-L-aspartate), followed by further stearoyl introduction into primary amine of PAsp(DET). With regard to the functionality of stearoyl PAsp(DET), the hydrophobic stearoyl moieties substantially increased the association number of siRNA and the polymer in their complexes, and also improved the complex stability in culture media containing serum, compared to PAsp(DET) without stearoylation. In addition, the PAsp(DET) backbone provides the excellent ability of endosome destabilization through pH-sensitive conformational change of the flanking 1, 2-diaminoethane moiety, allowing efficient, but less toxic, endosomal escape (Miyata et al., 2008). Consequently, the hydrophobized cationic polymer achieved significant silencing *in vitro* against a cancer-related gene, vascular endothelial growth factor (VEGF), as well as a reporter gene, indicating that stearoyl PAsp(DET) is a promising platform for *in vivo* siRNA delivery.

Toward *in vivo* application of stearoyl PAsp(DET), an additional modification is necessary to compromise its undesired binding with blood components. Hence, poly(ethylene gylcol) (PEG) was selected to improve the biocompatibility of nanoparticles in the bloodstream. Modification with PEG creates a barrier layer around the siRNA complexes allowing them to evade adhesion to blood components and elimination by the reticuloendothelial system (Owens & Peppas, 2006, Nomoto et al., 2011). On the other hand, presence of such PEG corona has disadvantages; it inhibits cellular uptake and endosomal escape of the siRNA complexes, leading to a substantial decrease in the gene silencing efficiency (Itaka & Kataoka, 2009). The development of environment-sensitive smart polymers could solve this PEG dilemma as they can detach the PEG segment from the siRNA complex in response to changes in environmental pH or redox potential (Lee & Kataoka, 2009). Disulfide linkage has been extensively utilized to prepare such smart polymers and their complexes with plasmid DNA and siRNA (Soundara Manickam & Oupický, 2006, Takae et al., 2008, Matsumoto et al., 2009, Park et al., 2010). This is based on the fact that several membrane proteins possess disulfide-thiol interchange activity and the concentration of reduced glutathione (GSH) is 50–1000 times higher than that of oxidized glutathione in cells (Jones et al., 2000, Morré & Morré, 2003). Thus, the disulfide linkage can be selectively cleaved on the cytoplasmic/endosomal membrane or in intracellular compartments. Furthermore, the GSH level is elevated in various human cancer tissues including breast, colon, and lung (Balendiran et al., 2004), indicating that the disulfide linkage can be selectively cleaved in such tumor tissues.

In the present study, we developed a block copolymer of stearoyl PAsp(DET) with PEG through a disulfide linkage (stearoyl PEG-SS-PAsp(DET)) to construct a smart siRNA complex, which can detach the PEG palisade in or around tumor cells. The siRNA complex with stearoyl PEG-SS-PAsp(DET) was physicochemically characterized in comparison with a non-detachable PEG control to reveal the effects of the reductive environment-sensitivity. Endogenous gene silencing efficacy was also compared between redox-sensitive and insensitive complexes in cultured cells. The circulating behavior of the stearoyl PEG-SS-PAsp(DET) complex in the bloodstream was observed using an intravital real-time confocal laser scanning microscope (IVRT-CLSM). Finally, the stearoyl PEG-SS-PAsp(DET) complex used for systemic siRNA delivery in a subcutaneous pancreatic BxPC3 tumor to demonstrate the *in vivo* gene silencing activity of the complex and its potential for cancer treatment based on an antiangiogenic approach with siRNA targeting VEGF (Holmes et al., 2007).

Materials and methods

Materials

β-Benzyl-L-aspartate *N*-carboxy-anhydride (BLA-NCA) was purchased from Chuo Kaseihin Co., Inc. (Tokyo, Japan). α-Methoxy-ω-mercapto PEG (PEG-SH, M_n = 10,000) and α-methoxy-ω-amino PEG (PEG-NH_2, M_n = 12,000) was obtained from NOF Co., Ltd. (Tokyo, Japan). *N, N*-Dimethylformamide (DMF), hexane, ethyl acetate, 2-aminoethanethiol, dichloromethane (DCM), *N*-hydroxysuccinimide (NHS), diethylether, *N*-methyl-2-pyrrolidone (NMP), ethanol, diethylenetriamine (DET), glucose, methanol (MeOH), and sodium hydrogen carbonate ($NaHCO_3$) were purchased from Wako Pure Chemical Industries, Ltd. (Osaka, Japan). RPMI-1640, glutathione (GSH), stearic acid, and diisopropylethylamine (DIPEA) were purchased from Sigma-Aldrich Co. (St. Louis, MO). 1-Ethyl-3-(3-dimethylaminopropyl)-carbodiimide, hydrochloride (EDC) was purchased from Dojindo (Kumamoto, Japan). DMF, NMP, and DIPEA were distilled with the conventional methods before use.

Human pancreatic adenocarcinoma cell line, BxPC3, was obtained from the American Type Culture Collection (Manassas, VA). Fetal bovine serum (FBS), sodium pyruvate, and Hanks buffer were purchased from Invitrogen (Carlsbad, CA). BALB/c nude mice were purchased from Charles River Japan (Kanagawa, Japan). Firefly luciferase siRNA (sense: 5′-CUU ACG CUG AGU ACU UCG AdTdT-3′; antisense: 5′-UCG AAG UAC UCA GCG UAA GdTdT-3′), Cy5-labeled firefly luciferase siRNA, Cy3-labeled firefly luciferase siRNA, scramble siRNA (sense: 5′-UUC UCC GAA CGU GUC ACG UdTdT-3′; antisense: 5′-ACG UGA CAC GUU CGG AGA AdTdT-3′ (Li et al., 2008)), VEGF siRNA (sense: 5′-GGA GUA CCC UGA UGA GAU CdTdT-3′; antisense: 5′-GAU CUC AUC AGG GUA CUC CdTdT-3′) were synthesized by Hokkaido System Science Co., Ltd. (Hokkaido, Japan). All fluorescent dyes were attached to 5′-end of sense stands.

Synthesis

Synthesis methods are available in Supplementary data.

Zeta potential measurement in reducing condition

Stearoyl PEG-SS-PAsp(DET) and stearoyl PEG-PAsp(DET) were separately dissolved in 50% ethanol solution (ethanol/10 mM HEPES buffer, pH = 7.3, 1:1 v/v) and then mixed with 20 μM siRNA solution (10 mM HEPES buffer, pH = 7.3) to form siRNA complexes (10 μM siRNA) at a N/P ratio of 5.0. The N/P ratio is defined as the residual molar ratio of the total amines in PAsp(DET) segment (N) to the phosphates in siRNA (P). The siRNA complexes were incubated at 4°C for 1 h and dialyzed against 10 mM HEPES buffer (pH = 7.3) overnight to obtain siRNA complexes (finally adjusted to 5 μM siRNA). For measurement of disulfide bond cleavage, siRNA complexes were mixed with pre-determined concentrations of GSH and incubated for 1 h at room temperature. Zeta potential was determined in a folded capillary cell (Malvern Instrument, Worcestershire, UK) using a Zetasizer (Malvern Instrument) at a temperature of 25°C.

Erythrocyte aggregation assay

Fresh blood from a rabbit was purchased from ProteinPurify Ltd. (Gunma, Japan) and erythrocytes were collected by centrifugation (3000 rpm, 10 min) to remove plasma and white blood cells. Erythrocytes were washed with PBS three times and suspended in PBS. siRNA complexes solutions (N/P = 5, 5 μM siRNA, 100 μL) prepared with stearoyl PEG-PAsp(DET), stearoyl PEG-SS-PAsp(DET), and stearoyl PAsp(DET) were mixed with 2× Hanks buffer (100 μL), then mixed with erythrocyte solution (100 μL) and incubated for 1 h at 37°C. The erythrocytes were observed with an optical microscope (Olympus, Tokyo, Japan) (Akagi et al., 2007).

Hemolytic activity assay

Fresh rabbit erythrocytes were washed three times with PBS and diluted with PBS at different dilution ratio. Each siRNA complex (N/P = 5, 5 μM siRNA, 20 μL) was first mixed with 2× Hanks buffer (20 μL), then immediately combined with a diluted erythrocyte solution (20 μL). The mixtures were incubated for 1 h at 37°C and centrifuged at 4000 rpm at 5 min to obtain supernatant containing released hemoglobin (Al-Badri et al., 2008). The concentration of hemoglobin was measured at OD_{414}. The 1% Triton X-100 (ICN Biomedicals Inc., Aurora, Ohio) and 10 mM HEPES buffer (pH = 7.3) solutions were used as references for 100% and 0% hemolysis, respectively.

Quantification of VEGF endogenous gene silencing by real-time PCR

BxPC3 cells were seeded into a 6-well plate at a density of 800,000 cells/well in RPMI-1640 containing 10% FBS, 2.2 g/L $NaHCO_3$, and 10 mL/L sodium pyruvate (RPMI/FBS). Before siRNA administration, the medium in each well was exchanged with fresh RPMI/FBS media. VEGF or scramble siRNA complexes (N/P = 5) were transfected at the desired siRNA concentration. After 48-h incubation, total RNAs in the cells were collected with an RNeasy Mini kit (Qiagen, Valencia, CA). Reverse transcription PCR was carried out using a QuantiTect Reverse Transcription kit (Qiagen) and real-time PCR was performed using a QuantiTect SYBR Green PCR kit (Qiagen) with an ABI 7500 Fast Real-Time PCR System (Applied Biosystems, Foster City, CA). All procedures followed the manufacturer's protocol. VEGF was amplified using 5′-AGT GGT CCC AGG CTG CAC-3′ as the forward primer and 5′-TCC ATG AAC TTC ACC ACT TCG T-3′ as the reverse primer. Actin was amplified using 5′-CCT GGC ACC CAG CAC AAT G -3′ as the forward primer and 5′-CGC CGA TCC ACA CGG AGT A -3′ as the reverse primer. All the experiments were performed in triplicate and data were normalized to actin expression.

Flow cytometer measurement

BxPC3 cells were seeded onto a 6-well plate at a density of 200,000 cells/well in RPMI/FBS. Cy5-labeled siRNA complexes were prepared from each polymer (N/P = 5) and transfected at 500 nM siRNA. After 4-h incubation, the media were removed and the cells were washed with 0.5 mL of PBS. The cells were treated with a trypsin-EDTA solution for 5 min and suspended in PBS. The intracellular uptake of the siRNA complexes was measured using a BD™ LSR II flow cytometer (BD Bioscience).

Cell viability assay

Cell viability was determined using a Cell Counting Kit-8 (Dojindo, Japan). BxPC3 cells were seeded onto a 96-well plate at a density of 5000 cells/well in RPMI/FBS. After overnight incubation, siRNA complexes (N/P = 5) were transfected, and cells were then incubated for 48 h. The growth medium was exchanged with fresh media (100 μL) containing the manufacturer's reagent (10 μL), and the cells were then incubated for 1.5 h. The absorbance of the media was measured at 450 nm using a microplate reader (Biorad, Hercules, CA).

Quantification of blood circulation of siRNA complex using intravital real-time confocal microscope

BALB/c nude mice (female, 6–8 weeks old) were anaesthetized with 2.5% isoflurane (Abbott Japan, Tokyo, Japan) using a Univenter 400 Anaesthesia Unit (Univentor, Lidingo, Sweden) and placed directly onto a thermoplate (Tokai Hit, Shizuoka, Japan). For each analysis, a cover slip (Muto Pure Chemicals Co., LTD, Tokyo, Japan) was placed on top of one ear with just enough pressure to flatten the ear. Image acquisition was carried out using a Nikon A1R confocal laser scanning microscope (CLSM) system attached to an upright ECLIPSE FN1 microscope (Nikon, Tokyo, Japan) (Matsumoto et al., 2010). The A1R incorporates a conventional galvano scanner and a high-speed resonant scanner with an acquisition speed of 30 frames/s and 512×512 resolution. Cy5-labeled siRNA complexes with each polymer (50 μg siRNA/mouse) were administered intravenously and detected with a He-Ne laser (640 nm excitation) and use of appropriate filters for Cy5 emission. Recorded images were analyzed by software (NIS-Elements AR, Nikon) to obtain time-dependent fluorescence intensity of Cy5.

Antitumor activity against subcutaneous BxPC3 tumor model

BALB/c nude mice (female, 7 weeks old) were subcutaneously implanted with BxPC3 tumor (3 mm × 3 mm × 1 mm). Two weeks later, mice with similar volume of tumor were randomly divided into three groups (n = 10). PEG-SS-PAsp(DET)/siRNA complexes (N/P = 5) prepared from scramble or VEGF siRNA (100 μg siRNA/mouse) and 10 mM HEPES buffer (pH = 7.3) were administered intravenously every three day (total 6 injections/mouse). An osmotic pressure of each solution was adjusted to a physiological condition with glucose at the final concentration of 5% (w/v ratio). Xenograft tumors were measured externally every alternate day and tumor volume was calculated by the following equation;

$$\text{Tumor volume} = (a \times b^2)/2$$

where a is the length of the major axis and b is the length of the minor axis. Relative tumor volume at each day was normalized by tumor volume at day 0. All animal experiments were carried out in accordance with the guidelines for animal experiments at the University of Tokyo, Japan.

Results and discussion

Synthesis of stearoyl PEG-PAsp(DET) and stearoyl PEG-SS-PAsp(DET)

PEG-SS-PAsp(DET), synthesized as previously described, was confirmed to show a narrow molecular weight distribution (Mw/Mn = 1.04) by gel permeation chromatography (Takae et al., 2008). PEG-PAsp(DET) and PAsp(DET) homopolymer were also prepared as controls (the synthesis procedures are described in Supplementary Information). The degree of polymerization (DP) of PAsp(DET) segment in these polymers was determined to be approximately 100 by ^{1}H NMR measurement. Stearoyl introduction was achieved by amide bond formation between *N*-succinimidyl octadecanoate and the primary amine of PAsp(DET) segments as previously described (Figure 1) (Kim et al., 2010). Stearoyl introduction ratio was targeted at 20%, from our previous findings that showed 20% stearoyl introduction into homopolymer PAsp(DET) achieved the best *in vitro* gene silencing (Kim et al., 2010). Successful preparation of each polymer with stearoyl introduction was confirmed by the peak intensity ratio between the methyl protons of stearoyl moieties (CH_3-, δ = 0.87 ppm) to β-protons of aspartate groups in PAsp(DET) (-CH_2-, δ = 2.89 ppm) in ^{1}H NMR spectra. A representative ^{1}H NMR chart of stearoyl PEG-SS-PAsp(DET) is provided in Supplementary Information (Figure S1). Detailed information for the three polymers obtained, such as DP, molecular weight of PEG, and stearoyl introduction ratio, are summarized in Table 1.

Formation of siRNA complex and physicochemical characterization

The formation of siRNA complexes with stearoyl PEG-PAsp(DET) and stearoyl PEG-SS-PAsp(DET) was investigated as a function of N/P ratio. The N/P ratio is defined

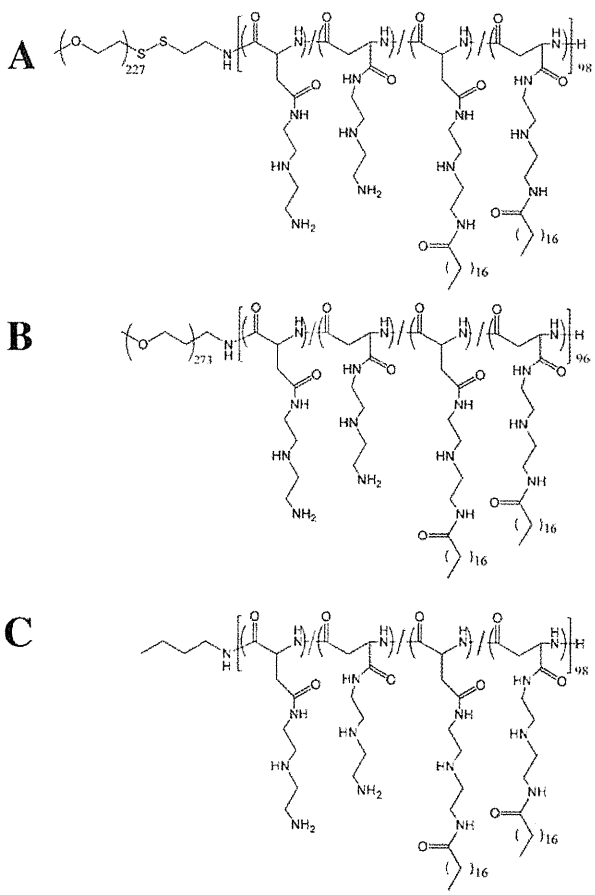

Figure 1. Chemical structures of stearoyl PEG-SS-PAsp(DET) (A), stearoyl PEG-PAsp(DET) (B), and stearoyl PAsp(DET) (C).

Table 1. Characterization of polymers.

	DP of PAsp (DET)	PEG weight	Stearoyl introduction ratio by ^{1}H NMR
Stearoyl PEG-PAsp(DET)	96	12,000	21%
Stearoyl PEG-SS-PAsp(DET)	98	10,000	20%
Stearoyl PAsp(DET)	98	·	20%

Table 2. Size and zeta potential of siRNA complexes.

	Size (nm) ± S.D.	Zeta Potential (mV) ± S.D.
Stearoyl PEG-PAsp(DET)	120±6	6.5±8.9
Stearoyl PEG-SS-PAsp(DET)	137±8	6.9±3.7
Stearoyl PAsp(DET)	176±7	35.0±6.6

as the residual molar ratio of the total amines in the PAsp(DET) segment (N) to the phosphates in siRNA (P). Note that stearoyl introduction concurrently reduces the number of primary amines (N) in the PAsp(DET) segment. Thus, the total amines in the PAsp(DET) segment after stearoylation do not include the primary amines of PAsp(DET), which are converted to amide bonds after stearoyl introduction. Formation of siRNA complexes at increasing N/P ratios was evaluated by gel electrophoresis (Figure S2). Complete disappearance of free siRNA and smear bands was observed between N/P=3 and 5 for both stearoyl PEG-PAsp(DET) and stearoyl PEG-SS-PAsp(DET), indicating that all siRNA molecules were associated with the block copolymer. Thus, N/P=5 was selected as the mixing ratio for the following experiments.

The size and zeta potential of siRNA complexes formed with stearoyl PEG-PAsp(DET), stearoyl PEG-SS-PAsp(DET), and stearoyl PAsp(DET) were determined by dynamic light scattering (DLS) and electrophoretic mobility measurements, respectively, and the results are summarized in Table 2. The sizes of siRNA complexes with stearoyl PEG-PAsp(DET) and stearoyl PEG-SS-PAsp(DET) ranged between 120 and 140 nm, and the zeta potentials were approximately 6.5 mV, indicating that both siRNA complexes prepared by the block copolymers have similar physicochemical characteristics. The zeta potential of siRNA complexes with the block copolymers was considerably lower than that of siRNA complex with stearoyl PAsp(DET) (35.0±6.6 mV), demonstrating that PEG shielding effectively reduced the surface charge of siRNA complexes to almost neutral through the formation of core-shell structured micelles.

The cleavage of disulfide bonds present in stearoyl PEG-SS-PAsp(DET)/siRNA complexes under reducing conditions was investigated by zeta potential measurement (Figure 2). Note that as reported previously PEG-SS-PAsp(DET) was cleaved into two segments of PEG and PAsp(DET) in the presence of 10 mM DTT measured by size exclusion chromatography, indicating that the disulfide bond between two segments is susceptible for cleavage under reducing conditions (Takae et al., 2008).

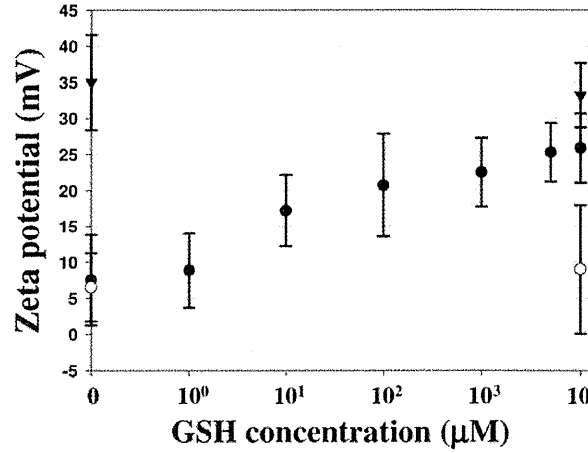

Figure 2. Disulfide reduction in siRNA complexes by GSH. Stearoyl PEG-SS-PAsp(DET) (•), stearoyl PEG-PAsp(DET) (○) and stearoyl PAsp(DET) (▼)/siRNA complexes were incubated with GSH for 1 h, followed by zeta potential analysis. Results are expressed as the mean ± S.D.

siRNA complexes (N/P=5) prepared from three types of cationers were incubated with varying concentrations of the reducing agent glutathione (GSH). siRNA complexes of stearoyl PEG-PAsp(DET) and stearoyl PAsp(DET) maintained their initial zeta potential even at 10 mM GSH and thereby indicated that they were inert to the reducing condition. In contrast, the zeta potential of stearoyl PEG-SS-PAsp(DET)/siRNA complex progressively increased with increasing concentrations of GSH and approximated to that of the stearoyl PAsp(DET)/siRNA complex. These results suggested that cationic PAsp(DET) segments are gradually exposed on the complex surface through PEG detachment as the disulfide bonds are cleaved. In addition, a significant increase in the zeta potential was observed at GSH concentrations more than 10 μM and the zeta potential value reached +26 mV at 10 mM GSH, indicating the potential ability of stearoyl PEG-SS-PAsp(DET)/siRNA complex to effectively detach PEG from the complex in the cytoplasm, where the concentration of GSH is 1–10 mM, and also to slightly detach it in murine plasma (GSH concentration=8.6±2.2 μM) (Navarro et al., 1999, Jones et al., 2000).

Erythrocyte aggregation and hemolytic assays

To investigate biocompatibility of siRNA complexes against blood components, an erythrocyte aggregation assay was performed. Erythrocytes have negatively charged surfaces and can interact with positively charged siRNA complexes. Thus, this assay serves as a simplified model to estimate the behavior of siRNA complex in the blood (Akagi et al., 2007). Erythrocytes purified from rabbit blood were incubated in Hanks buffer (pH=7.3) containing siRNA complexes prepared from each of the three polycations for 1 h at 37°C (Figure 3A–D). Erythrocytes were not observed after incubation with the stearoyl PAsp(DET)/siRNA complex, indicating that the

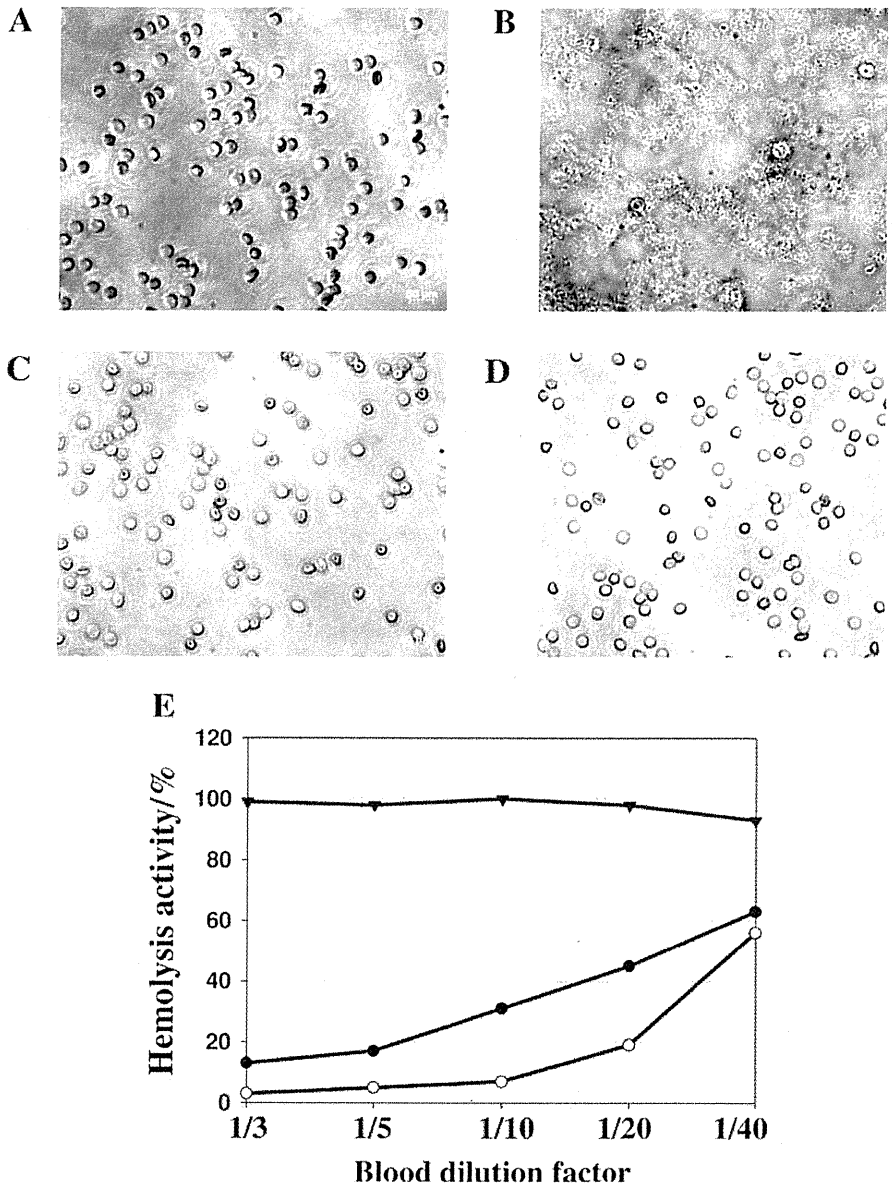

Figure 3. Erythrocyte aggregation and hemolytic activity assays of three different siRNA complexes. Optical images of rabbit erythrocytes mixed with HEPES buffer (pH = 7.3, panel A) and siRNA complexes (N/P = 5) of stearoyl PAsp(DET) (panel B), stearoyl PEG-PAsp(DET) (panel C), and stearoyl PEG-SS-PAsp(DET) (panel D). (E) Hemolytic activity of siRNA complexes against rabbit erythrocytes. Diluted erythrocytes were mixed with siRNA complexes of stearoyl PAsp(DET) (▾), stearoyl PEG-PAsp(DET) (○), and stearoyl PEG-SS-PAsp(DET) (•) for 1 h and then the released hemoglobin was measured at OD_{414}. Blood dilution factor means how much erythrocyte solution was diluted by PBS, and was calculated from the following equation: Dilution factor = [volume of collected blood] / ([volume of collected blood] + [volume of added PBS]).

erythrocytes were completely disrupted by the stearoyl PAsp(DET) complex (Figure 3B). In contrast, erythrocytes incubated with stearoyl PEG-PAsp(DET) and stearoyl PEG-SS-PAsp(DET)/siRNA complexes maintained their original shapes, indicating that the restricted surface charge and sterical repulsion of PEG corona effectively prevented interaction between the siRNA complexes and erythrocytes. (Figure 3C and D).

The biocompatibility of siRNA complexes was further quantitatively investigated by a hemolytic assay, which measures the amount of hemoglobin released from disrupted erythrocytes (Figure 3E). Stearoyl PAsp(DET)/siRNA complex exhibited almost 100% hemolytic activity at all the tested erythrocyte concentrations. Note that PAsp(DET) without the stearoyl moiety had negligible hemolytic activity. Thus, the severe hemolysis due to stearoyl PAsp(DET) may be because of its cationic detergent-like structure, in which a long hydrophobic chain is attached to a positively charged head group, rather than the inherent polycationic nature of PAsp(DET).

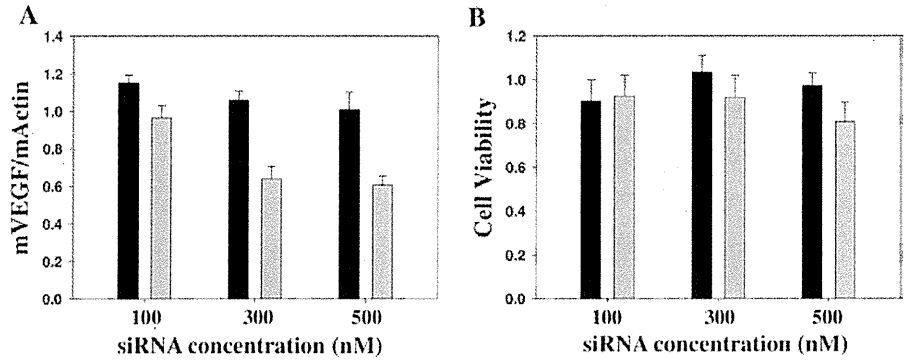

Figure 4. Endogenous gene silencing of siRNA complexes with two types of PEG block copolymers measured by real-time PCR (A). Comparison of siRNA complexes (N/P = 5) of stearoyl PEG-PAsp(DET) (black) and stearoyl PEG-SS-PAsp(DET) (gray) for VEGF gene in BxPC3 cells. Each sample was transfected in the BxPC3 cells for 48 h. The VEGF mRNA amount was normalized with actin mRNA as an internal control. Results are expressed as the mean ± S.D. (n = 3). Viability of BxPC3 cells treated with each siRNA complex (N/P = 5) of stearoyl PEG-PAsp(DET) (black) and stearoyl PEG-SS-PAsp(DET) (gray) under the same experimental condition as the real-time PCR (B). Results are expressed as the mean ± S.D. (n = 4).

Meanwhile, both siRNA complexes of stearoyl PEG-PAsp(DET) and stearoyl PEG-SS-PAsp(DET) exhibited considerably less hemolytic activity. From these results, the reduced interaction between siRNA complexes and blood components owing to PEGylation was quantitatively confirmed, thus demonstrating that the PEG palisade is essential for *in vivo* siRNA delivery.

Endogenous gene silencing in cultured cells

The potential of VEGF gene silencing in BxPC3 cells toward potential antiangiogenic cancer treatment was compared with siRNA complexes from stearoyl PEG-PAsp(DET) and stearoyl PEG-SS-PAsp(DET) (Figure 4A). VEGF or scramble siRNA complexes (N/P = 5) were transfected for 48 h, and then the amounts of VEGF mRNA were measured by real-time PCR with normalization by actin mRNA. VEGF gene silencing efficacy was shown with further normalization by the amount of VEGF mRNA treated by scramble siRNA. Stearoyl PEG-PAsp(DET) did not show significant VEGF gene silencing in the range 100–500 nM siRNA. In contrast, stearoyl PEG-SS-PAsp(DET) exhibited significant VEGF gene silencing around 40% at 300 nM and 500 nM siRNA. The enhanced gene silencing efficacy of stearoyl PEG-SS-PAsp(DET) was investigated with respect to cellular uptake by flow cytometry. A 4-h incubation (at 500 nM siRNA) revealed that the cellular uptake of stearoyl PEG-SS-PAsp(DET)/siRNA complex was two times higher than that of stearoyl PEG-PAsp(DET)/siRNA complex (data not shown), indicating that the higher cellular uptake of siRNA could be one of the reasons for the enhanced gene silencing activity of stearoyl PEG-SS-PAsp(DET). The different cellular uptake amount between detachable and non-detachable PEG systems may occur by the cleavage of some fractions of disulfide bonds in the detachable PEG system in the cell culture media. Indeed, a recent study revealed that the disulfide linkage between DNA nanoparticles and their surface PEG could be cleaved by extracellular free thiols (30–180 μM) secreted by cancer cells in culture conditions (Sun & Davis, 2010). However, this characteristic cannot completely explain the significantly higher gene silencing efficacy of stearoyl PEG-SS-PAsp(DET). PEG detachment in the endosome through the cleavage of the disulfide linkage has been reported and the degradation of disulfide bonds in polymers was observed in cytoplasm, leading to higher plasmid DNA transfection efficacy (Takae et al., 2008, Meng et al., 2009). Therefore, several mechanisms, including higher cellular uptake, may play a role in the enhanced gene silencing efficacy of stearoyl PEG-SS-PAsp(DET).

Low cytotoxicity is a prerequisite for the development of a systemic siRNA delivery carrier. Thus, cell viability of BxPC3 cells following administration of siRNA complexes with stearoyl PEG-PAsp(DET) and stearoyl PEG-SS-PAsp(DET) was measured by a MTT assay (Figure 4B). Cell viabilities were more than 80%, even at siRNA concentration of 500 nM, indicating that both block copolymer complexes were not severely cytotoxic to BxPC3 cells.

Blood circulation properties of stearoyl PEG-SS-PAsp(DET)/siRNA complexes

The behavior of the siRNA complex with stearoyl PEG-SS-PAsp(DET) in the bloodstream was observed using IVRT-CLSM, and investigated in terms of blood circulation. Naked siRNA and PEG-SS-PAsp(DET)/siRNA complex without stearoyl modification were also observed as controls. Each sample prepared from Cy5-labeled siRNA was injected intravenously at a dose of 50 μg siRNA/mouse into a tail vein, and then a vein in the earlobe was observed to detect fluorescence of Cy5-labeled siRNA in the bloodstream. The images observed were analyzed to obtain the time-dependent fluorescence intensity of Cy5-labeled siRNA in the vein and tissues (Figure S3). Fluorescence intensities were normalized with background fluorescence in the vein before injection (0%) and the highest fluorescence

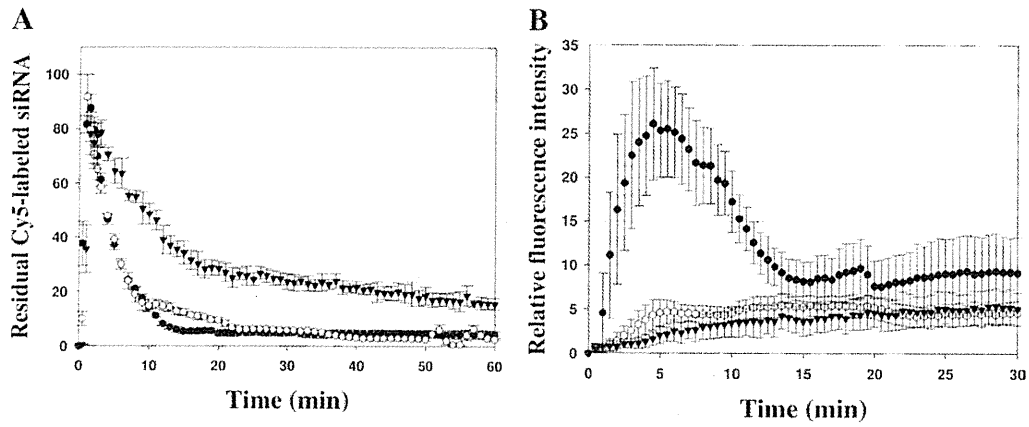

Figure 5. Behavior of siRNA complexes in the bloodstream observed by IVRT-CLSM. Naked Cy5-labeled siRNA (•) and Cy5-labeled siRNA complexes (N/P = 5) of PEG-SS-PAsp(DET) (○) and stearoyl PEG-SS-PAsp(DET) (▾) were administered intravenously at a dose of 50 μg siRNA/mouse. A vein in the earlobe was observed by a confocal microscope and recorded images were analyzed by a software. (A) Residual fluorescence intensity of Cy5-labeled siRNA in a vein and (B) relative fluorescence intensity of Cy5-labeled siRNA in tissues. Fluorescence was analyzed in more than five regions in the image and results are expressed as the mean ± S.D.

of the vein in the initial period after injection (100%) (Figure 5A and B).

Vein fluorescence in naked Cy5-labeled siRNA was almost same as the background value within 10 min of the injection, indicating the rapid elimination of naked siRNA from the bloodstream. The tissue fluorescence of naked Cy5-labeled siRNA increased considerably until 5 min, decreased until 15 min after the injection, and then reached a plateau. As a macromolecular nucleotide, rapid extravasation of siRNA (Mw = 13,300) into the tissue within 5 min would be difficult; therefore, the initial increase in fluorescence was probably because of Cy5-labeled siRNA being quickly degraded in the bloodstream allowing the released Cy5 dyes to diffuse into the tissue. The subsequent decrease in fluorescence may be because of the suspended supply of Cy5 dyes from the vein and the escape of Cy5 dyes from tissues into lymphatic vessels. On the other hand, the vein fluorescence of stearoyl PEG-SS-PAsp(DET)/siRNA complex decreased more slowly than that of the naked siRNA or the PEG-SS-PAsp(DET)/siRNA complex, indicating that the hydrophobically stabilized complex exerted the longevity of siRNA in the bloodstream. In addition, siRNA complex formation showed a pronounced effect on the fluorescence intensity in the tissue; the initial increase in fluorescence, as seen in naked siRNA, was substantially suppressed by siRNA complex formation. This indicated that a large portion of Cy5-labeled siRNA molecules were yet to be complexed in the bloodstream, at least in the initial period and also that those siRNAs should be protected from enzymatic degradation. Notably, the stearoyl system achieved the highest fluorescence in the vein at 60 min and the lowest fluorescence in the tissue within 20 min of the intravenous injection. Thus, stearoyl modification appears to stabilize siRNA complex even in the bloodstream.

Systemic administration of siRNA complexes into a subcutaneous BxPC3 tumor

To verify whether *in vivo* gene silencing can be obtained by systemic siRNA delivery with stearoyl PEG-SS-PAsp(DET), VEGF siRNA and its complexes were used to treat a xenograft BxPC3 tumor, and then the VEGF mRNA level in the tumor tissue was determined by real-time PCR. One day after the injection (50 μg siRNA/mouse) of naked VEGF siRNA, stearoyl PEG-SS-PAsp(DET)/scramble siRNA complex, stearoyl PEG-SS-PAsp(DET)/VEGF siRNA complex, and PEG-SS-PAsp(DET)/VEGF siRNA complex (N/P = 5), total RNAs were extracted from the tumor tissue and the amount of VEGF mRNA was measured relative to actin mRNA as a house-keeping gene (Figure 6A). Only the stearoyl PEG-SS-PAsp(DET)/VEGF siRNA complex showed significant VEGF mRNA reduction (around 40%) in the tested samples ($p < 0.05$). This VEGF mRNA reduction was confirmed to be the siRNA sequence specific effect because the significant mRNA reduction was not induced by the scramble siRNA complex with stearoyl PEG-SS-PAsp(DET). In addition, the less stable siRNA complex with PEG-SS-PAsp(DET) as well as naked VEGF siRNA did not exhibit VEGF gene silencing in the tumor, indicating that the improved longevity of siRNA in the bloodstream may be essential for systemic delivery of siRNA to the tumor tissue (Figure 5A and B).

The potential antitumor activity of stearoyl PEG-SS-PAsp(DET) complexes was investigated against the xenograft BxPC3 tumor. VEGF was selected as the target gene to inhibit angiogenesis in tumor tissues (Holmes et al., 2007). VEGF or scramble siRNA complexes formed by stearoyl PEG-SS-PAsp(DET) (N/P = 5) and HEPES buffer were administered intravenously into mice having a subcutaneous BxPC3 tumor. Each mouse was given six injections with 100 μg siRNA per injection, and the

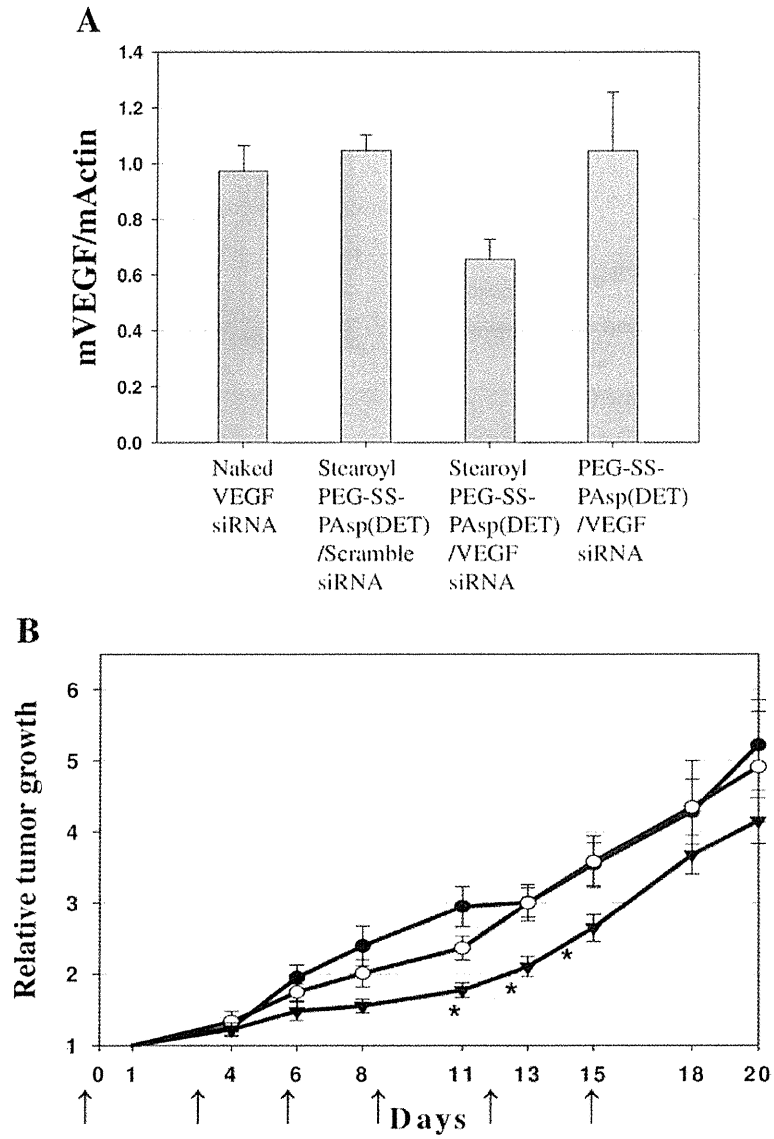

Figure 6. VEGF mRNA level in BxPC3 tumor measured by real-time PCR (A). Each tumor was excised 24 h after the sample injection. The VEGF mRNA amount was normalized with actin mRNA as an internal control. Results are expressed as the mean ± S.D. (n = 3). Subcutaneous BxPC3 tumor growth in the treatment of siRNA formed with stearoyl PEG-SS-PAsp(DET) (N/P = 5) (B). The mice were intravenously injected with siRNA complexes (100 μg siRNA/mouse) and HEPES buffer every three days. Tumor growths treated by scramble siRNA (○), VEGF siRNA (▼), and HEPES buffer (•) were measured externally every alternate day. Error bar means standard error. Statistical significance: $^{*}p < 0.05$.

tumor size was measured externally every alternate day (Figure 6B). VEGF siRNA delivered by stearoyl PEG-SS-PAsp(DET) significantly inhibited the tumor growth between 11 and 15 days, compared to HEPES buffer- or scramble siRNA complex-treated tumors, consistent with the results of VEGF mRNA reduction (Figure 6A). Thereafter, tumor growth inhibition by the VEGF siRNA complex was gradually lost after siRNA injection was suspended. To our knowledge, few groups have successfully obtained antiangiogenesis results with intravenous administration of VEGF or VEGF receptor-2 siRNA using polyethylenimine as delivery carriers (Schiffelers et al., 2004, Kim et al., 2008). Our study also demonstrated the significant antitumor activity of systemic delivery of the siRNA complex with the unique carrier design concept and the reductive-sensitive smart polymer.

Conclusions

Stearoyl PEG-SS-PAsp(DET) successfully formed a smart siRNA complex, which could detach from the surrounding PEG chains in response to environmental reductive potential. The siRNA complex exhibited efficient gene silencing *in vitro* with low cytotoxicity and improved

longevity in the bloodstream. Significant *in vivo* gene silencing was achieved in subcutaneous pancreatic tumor tissue by systemic administration of the VEGF siRNA complex. Repeated doses of the siRNA complex led to significant growth inhibition of the tumor, presumably because of the antiangiogenic effect of VEGF gene silencing. However, the growth inhibition of the tumor did not satisfy our expectations even in high dose amount of VEGF siRNA. Even though the longevity in the blood was improved in this study, the result was not enough to obtain the impressive antiangiogenic effect. The use of longer PEG chain or the introduction of targeting moiety will improve the pharmakinetics of the siRNA complex, which plan for next research. Overall, these results demonstrate the feasibility of the PEG-detachable, stable siRNA carrier for siRNA-based cancer treatment.

Acknowledgements

HJ Kim is thankful to Ms. Michiko Fujita for her help with the polymer synthesis.

Declaration of interest

This research is granted by the Japan Society for the Promotion of Science (JSPS) through the "Funding Program for World-Leading Innovative R&D on Science and Technology (FIRST Program)" initiated by the Council for Science and Technology Policy (CSTP) as well as Takeda Science Foundation.

References

Aagaard L, Rossi JJ. (2007). RNAi therapeutics: principles, prospects and challenges. Adv Drug Deliv Rev, 59, 75–86.

Dykxhoorn DM. (2009). RNA interference as an anticancer therapy: a patent perspective. Expert Opin Ther Pat, 19, 475–491.

He S, Zhang D, Cheng F, Gong F, Guo Y. (2009). Applications of RNA interference in cancer therapeutics as a powerful tool for suppressing gene expression. Mol Biol Rep, 36, 2153–2163.

Christie RJ, Nishiyama N, Kataoka K. (2010). Delivering the code: polyplex carriers for deoxyribonucleic acid and ribonucleic acid interference therapies. Endocrinology, 151, 466–473.

Fang J, Nakamura H, Maeda H. (2011). The EPR effect: Unique features of tumor blood vessels for drug delivery, factors involved, and limitations and augmentation of the effect. Adv Drug Deliv Rev, 63, 136–151.

Whitehead KA, Langer R, Anderson DG. (2009). Knocking down barriers: advances in siRNA delivery. Nat Rev Drug Discov, 8, 129–138.

HJ, Ishii A, Miyata K, Lee Y, Wu S, Oba M, Nishiyama N, Kataoka K. (2010). Introduction of stearoyl moieties into a biocompatible cationic polyaspartamide derivative, PAsp(DET), with endosomal escaping function for enhanced siRNA-mediated gene knockdown. J Control Release, 145, 141–148.

Miyata K, Oba M, Nakanishi M, Fukushima S, Yamasaki Y, Koyama H, Nishiyama N, Kataoka K. (2008). Polyplexes from poly(aspartamide) bearing 1,2-diaminoethane side chains induce pH-selective, endosomal membrane destabilization with amplified transfection and negligible cytotoxicity. J Am Chem Soc, 130, 16287–16294.

Owens DE 3rd, Peppas NA. (2006). Opsonization, biodistribution, and pharmacokinetics of polymeric nanoparticles. Int J Pharm, 307, 93–102.

Nomoto T, Matsumoto Y, Miyata K, Oba M, Fukushima S, Nishiyama N, Yamasoba T, Kataoka K. (2011). In situ quantitative monitoring of polyplexes and polyplex micelles in the blood circulation using intravital real-time confocal laser scanning microscopy. J Control Release, 151, 104–109.

Itaka K, Kataoka K. (2009). Recent development of nonviral gene delivery systems with virus-like structures and mechanisms. Eur J Pharm Biopharm, 71, 475–483.

Lee Y, Kataoka K. (2009). Biosignal-sensitive polyion complex micelles for the delivery of biopharmaceuticals. Soft Matter, 5, 3810–3817.

Soundara Manickam D, Oupický D. (2006). Polyplex gene delivery modulated by redox potential gradients. J Drug Target, 14, 519–526.

Park K, Lee MY, Kim KS, Hahn SK. (2010). Target specific tumor treatment by VEGF siRNA complexed with reducible polyethyleneimine-hyaluronic acid conjugate. Biomaterials, 31, 5258–5265.

Matsumoto S, Christie RJ, Nishiyama N, Miyata K, Ishii A, Oba M, Koyama H, Yamasaki Y, Kataoka K. (2009). Environment-responsive block copolymer micelles with a disulfide cross-linked core for enhanced siRNA delivery. Biomacromolecules, 10, 119–127.

Takae S, Miyata K, Oba M, Ishii T, Nishiyama N, Itaka K, Yamasaki Y, Koyama H, Kataoka K. (2008). PEG-detachable polyplex micelles based on disulfide-linked block catiomers as bioresponsive nonviral gene vectors. J Am Chem Soc, 130, 6001–6009.

Jones DP, Carlson JL, Mody VC, Cai J, Lynn MJ, Sternberg P. (2000). Redox state of glutathione in human plasma. Free Radic Biol Med, 28, 625–635.

Morré DJ, Morré DM. (2003). Cell surface NADH oxidases (ECTO-NOX proteins) with roles in cancer, cellular time-keeping, growth, aging and neurodegenerative diseases. Free Radic Res, 37, 795–808.

Balendiran GK, Dabur R, Fraser D. (2004). The role of glutathione in cancer. Cell Biochem Funct, 22, 343–352.

Holmes K, Roberts OL, Thomas AM, Cross MJ. (2007). Vascular endothelial growth factor receptor-2: structure, function, intracellular signalling and therapeutic inhibition. Cell Signal, 19, 2003–2012.

Li SD, Chono S, Huang L. (2008). Efficient oncogene silencing and metastasis inhibition via systemic delivery of siRNA. Mol Ther, 16, 942–946.

Akagi D, Oba M, Koyama H, Nishiyama N, Fukushima S, Miyata T, Nagawa H, Kataoka K. (2007). Biocompatible micellar nanovectors achieve efficient gene transfer to vascular lesions without cytotoxicity and thrombus formation. Gene Ther, 14, 1029–1038.

AL-Badri ZM, Som A, Lyon S, Nelson CF, Nüsslein K, Tew GN. (2008). Investigating the effect of increasing charge density on the hemolytic activity of synthetic antimicrobial polymers. Biomacromolecules, 9, 2805–2810.

Matsumoto Y, Nomoto T, Cabral H, Matsumoto Y, Watanabe S, Christie RJ, Miyata K, Oba M, Ogura T, Yamasaki Y, Nishiyama N, Yamasoba T, Kataoka K. (2010). Direct and instantaneous observation of intravenously injected substances using intravital confocal micro-videography. Biomed Opt Express, 1, 1209–1216.

Navarro J, Obrador E, Carretero J, Petschen I, Aviñó J, Perez P, Estrela JM. (1999). Changes in glutathione status and the antioxidant system in blood and in cancer cells associate with tumour growth in vivo. Free Radic Biol Med, 26, 410–418.

Sun W, Davis PB. (2010). Reducible DNA nanoparticles enhance *in vitro* gene transfer via an extracellular mechanism. J Control Release, 146, 118–127.

Meng F, Hennink WE, Zhong Z. (2009). Reduction-sensitive polymers and bioconjugates for biomedical applications. Biomaterials, 30, 2180–2198.

Kim SH, Jeong JH, Lee SH, Kim SW, Park TG. (2008). Local and systemic delivery of VEGF siRNA using polyelectrolyte complex micelles for effective treatment of cancer. J Control Release, 129, 107–116.

Schiffelers RM, Ansari A, Xu J, Zhou Q, Tang Q, Storm G, Molema G, Lu PY, Scaria PV, Woodle MC. (2004). Cancer siRNA therapy by tumor selective delivery with ligand-targeted sterically stabilized nanoparticle. Nucleic Acids Res, 32, e149.

nature nanotechnology

ARTICLES

PUBLISHED ONLINE: 23 OCTOBER 2011 | DOI: 10.1038/NNANO.2011.166

Accumulation of sub-100 nm polymeric micelles in poorly permeable tumours depends on size

H. Cabral[1], Y. Matsumoto[2], K. Mizuno[3], Q. Chen[4], M. Murakami[2], M. Kimura[2], Y. Terada[5], M. R. Kano[6], K. Miyazono[6,7], M. Uesaka[3,7], N. Nishiyama[2,7]* and K. Kataoka[1,2,4,7]*

A major goal in cancer research is to develop carriers that can deliver drugs effectively and without side effects. Liposomal and particulate carriers with diameters of ~100 nm have been widely used to improve the distribution and tumour accumulation of cancer drugs, but so far they have only been effective for treating highly permeable tumours. Here, we compare the accumulation and effectiveness of different sizes of long-circulating, drug-loaded polymeric micelles (with diameters of 30, 50, 70 and 100 nm) in both highly and poorly permeable tumours. All the polymer micelles penetrated highly permeable tumours in mice, but only the 30 nm micelles could penetrate poorly permeable pancreatic tumours to achieve an antitumour effect. We also showed that the penetration and efficacy of the larger micelles could be enhanced by using a transforming growth factor-β inhibitor to increase the permeability of the tumours.

Targeting tumours with long-circulating nanomedicines, such as poly(ethylene glycol)-modified liposomes and polymeric micelles[1–6], is a promising strategy in systemic cancer treatment. These materials accumulate in solid tumours through the enhanced permeability and retention (EPR) effect[7], which is characterized by leaky blood vessels and an impaired lymphatic drainage in tumour tissues[7]. Compared with free drug, nanomedicines accumulate in solid tumours more easily and selectively and therefore offer better antitumour activity[8–15]. Several nanomedicines, including Doxil and Abraxane (diameters of 90 and 130 nm, respectively), have shown significant antitumour activity in highly vascularized tumours such as Kaposi's sarcoma and breast cancer, and have been approved for clinical use[16,17]. However, because Doxil and other nanomedicines with diameters larger than 100 nm have shown limited penetration and accumulation in tumours with hypovascular and hypopermeable characteristics[18–20] (such as intractable pancreatic tumours[18,20]), nanomedicines in the sub-100 nm range are now regarded as being more important in the study of tumour penetration[21,22].

Polymeric micelles (self-assemblies of block copolymers) are promising long-circulating nanomedicines[5,6,8–10] and have been widely studied in preclinical and clinical trials[13,14,23]. Clinical studies have demonstrated that polymeric micelles of poly(ethylene glycol)–*b*-poly(amino acid) copolymers incorporating paclitaxel, SN-38, doxorubicin or cisplatin drugs can reduce the toxic side effects of the loaded drugs[13,14,24,25] while maintaining appreciable antitumour efficacy. Micelles containing paclitaxel and SN-38 have been reported to reduce the size of tumours in patients with advanced cancers of the breast and pancreas[13,14]. The dense poly(ethylene glycol) (PEG) shell of the micelles prevents protein adsorption and recognition by the phagocyte system, and this prolongs blood circulation, a prerequisite for enhanced tumour accumulation based on the EPR effect. Moreover, with these micelles, the size (including those in the sub-100 nm range), stability, loading capacity and release kinetics of the drugs can be modulated by engineering the constituent block copolymers[5,6]. Here, we examine whether a series of micellar nanomedicines that have diameters less than 100 nm and that carry the potent tumoricidal agent 1,2-diaminocyclohexane-platinum(II) (DACHPt) (the parent complex of oxaliplatin) can accumulate and penetrate poorly permeable pancreatic tumours. Our results show that the size of the nanomedicines critically affects the penetration and efficacy of the drugs in the tumours. Larger micelles that could not penetrate otherwise, could penetrate once the permeability of the tumours was improved by administering a transforming growth factor-β inhibitor.

Characterization of DACHPt-loaded micelles

DACHPt-loaded micelles (DACHPt/m) were spontaneously formed from the interaction of the platinum of DACHPt and the carboxylic moieties of PEG–*b*-poly(glutamic acid) (PEG–*b*-P(Glu)) copolymer and the poly(glutamic acid) (P(Glu)) homopolymer in water (Fig. 1a)[10,26,27]. Differently sized DACHPt/m were synthesized by controlling the mixing ratio of P(Glu) from the homopolymer and the P(Glu) portion of PEG–*b*-P(Glu) (Fig. 1b). As the ratio of P(Glu) in the homopolymer and P(Glu) in the copolymer increases, the size of the micelles increases. Thus, the size of DACHPt/m ranged from 30 nm without the addition of P(Glu) homopolymer to more than 100 nm, while maintaining a narrow distribution as determined by dynamic light scattering (DLS) measurements and transmission electron microscopy (TEM) observations (Table 1 and Supplementary Fig. S1, respectively). Note that DLS measurements provide the hydrodynamic diameter of the DACHPt/m, and TEM gives the core diameter of the micelles, so the difference between the hydrodynamic diameter and the core size gives an indication of the thickness of the PEG shell of the micelles.

[1]Department of Bioengineering, Graduate School of Engineering, The University of Tokyo, 7-3-1 Hongo, Bunkyo-ku, Tokyo, 113-8656, Japan, [2]Center for Disease Biology and Integrative Medicine, Graduate School of Medicine, The University of Tokyo, 7-3-1 Hongo, Bunkyo-ku, Tokyo 113-0033, Japan, [3]Department of Nuclear Engineering and Management, Graduate School of Engineering, The University of Tokyo, 7-3-1 Hongo, Bunkyo-ku, Tokyo 113-8656, Japan, [4]Department of Materials Engineering, Graduate School of Engineering, The University of Tokyo, 7-3-1 Hongo, Bunkyo-ku, Tokyo 113-8656, Japan, [5]SPring 8, JASRI, 1-1-1 Kouto, Sayo-cho, Sayo-gun, Hyogo 679-5198, Japan, [6]Department of Molecular Pathology, Graduate School of Medicine, The University of Tokyo, 7-3-1 Hongo, Bunkyo-ku, Tokyo 113-0033, Japan, [7]Center for NanoBio Integration (CNBI), The University of Tokyo, 7-3-1 Hongo, Bunkyo-ku, Tokyo 113-8656, Japan. *e-mail: nishiyama@bmw.t.u-tokyo.ac.jp; kataoka@bmw.t.u-tokyo.ac.jp

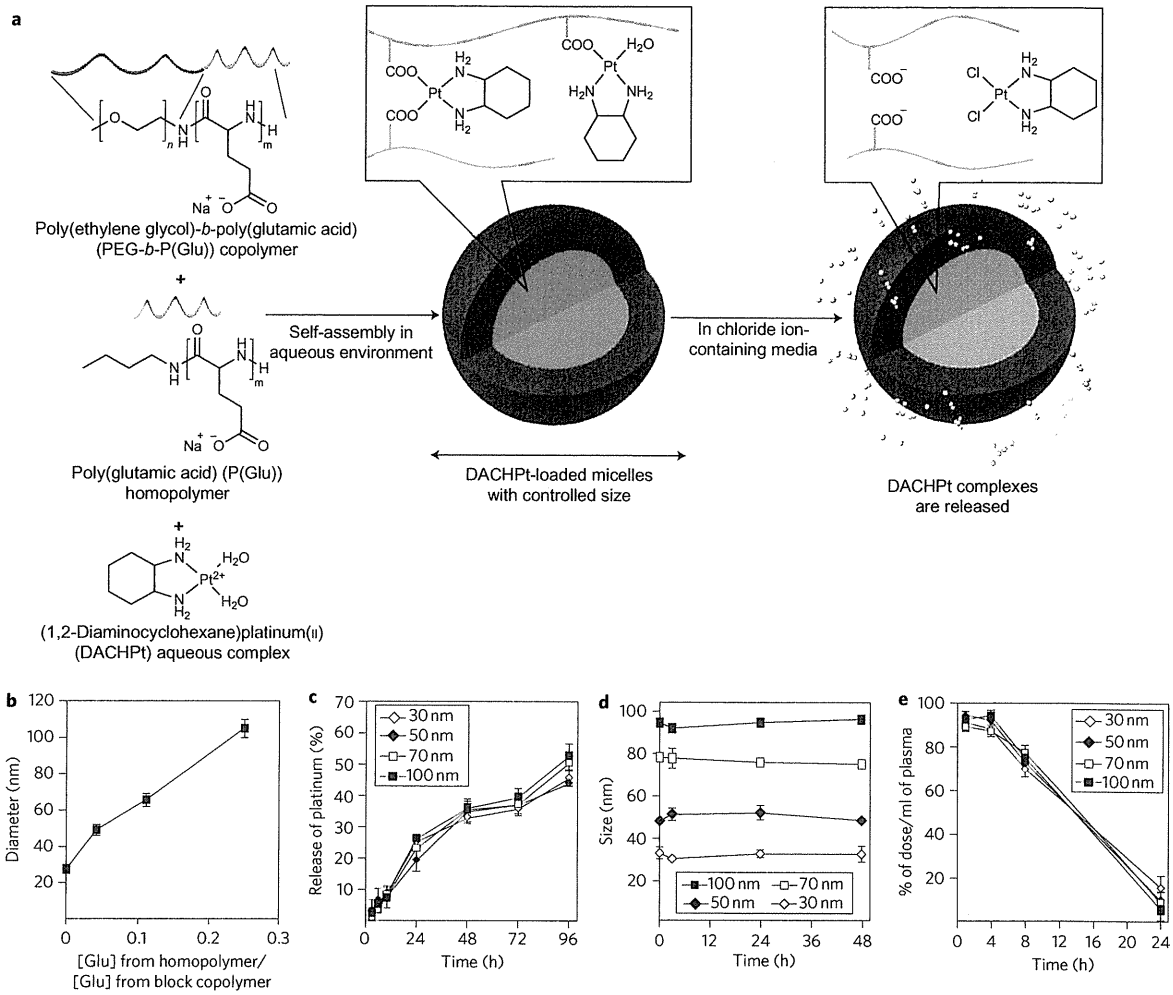

Figure 1 | Construction and physicochemical properties of DACHPt-loaded micellar nanomedicines (DACHPt/m) with different diameters. a, Schematic showing DACHPt/m formed through the interaction between DACHPt and the carboxylic groups of poly(glutamic acid) (green) in PEG-*b*-P(Glu) and P(Glu). In media containing chloride ions, DACHPt (yellow circles) is released from the micelles through ligand exchange between the carboxylic groups in P(Glu) and the chloride ions. **b**, Changing micelle size by altering the ratio of P(Glu) from the homopolymer and the P(Glu) portion of PEG-*b*-P(Glu) in the mixture. Total glutamic acid residue concentration was maintained at 5 mM. **c**, Micelles of all sizes release DACHPt at similar rates. **d**, Micelles of all sizes incubated in cell culture media containing 10% serum at 37 °C maintained their sizes over 48 h. **e**, Plasma clearances of micelles with different diameters follow similar trends. Data are means±s.e.m., $n = 3$.

Table 1 | Diameter, size distribution, drug loading and surface charge of 30, 50, 70 and 100 nm micelles.

Size (nm)*	Polydispersity index	[Pt]/[COO] (mol/mol)†	Pt/polymer (wt/wt%)	Zeta-potential (mV)‡
30	0.16	0.56	34	−2.29±1.41
54	0.14	0.6	48	−1.61±0.58
69	0.12	0.57	54	−0.89±0.33
110	0.11	0.52	69	0.15±0.21

*Determined by DLS. †Determined by ICP-MS (platinum concentration) and weight of micelles. ‡Determined by laser doppler electrophoresis ($n = 4$, mean±s.d.).

The 30, 50, 70 and 100 nm DACHPt/m presented similar zeta potentials, ranging from −2.29 to 0.15 mV at pH 7.4 (Table 1). These micelles showed similar drug release rates (Fig. 1c), driven by the ligand exchange of DACHPt between the carboxylic groups of P(Glu) and the chloride ions in the biological media. After 96 h incubation in cell culture media containing 10% fetal bovine serum (FBS) at 37 °C, the drug release from DACHPt/m reached ~50% (Fig. 1c). Under similar conditions, differently sized DACHPt/m maintained their diameters for over 48 h (Fig. 1d). DACHPt/m of different sizes also showed similar plasma clearance rates (~12% of injected dose (ID) per ml plasma remained after 24 h) and plasma half-lives (7–8 h) (Fig. 1e and Supplementary Table S1, respectively). We recently showed that DACHPt/m can maintain their micellar structure in the circulation for at least 24 h after injection[28]. Furthermore, DACHPt/m of varying sizes show similar distributions in the kidney, liver and spleen (Supplementary Fig. S2 and

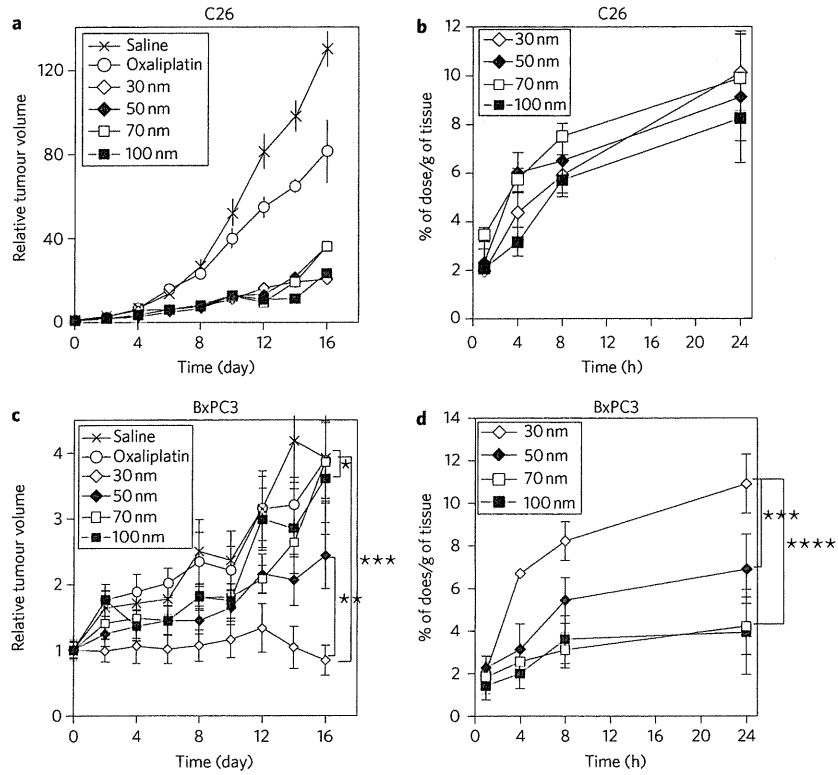

Figure 2 | Anticancer activity and tumour accumulation of DACHPt/m with different diameters. a-d, Plots of relative tumour volumes of subcutaneous hyperpermeable murine colon adenocarcinoma (C26) (**a**) and subcutaneous hypopermeable human pancreatic adenocarcinoma BxPC3 (**c**) tumours, and accumulation of DACHPt/m in C26 (**b**) and BxPC3 (**d**) tumours. To evaluate antitumour activity, oxaliplatin was injected on days 0, 2 and 4 (dose, 8 mg kg^{-1}) and micelles were injected on days 0, 2 and 4 (dose, 3 mg kg^{-1} on a platinum basis). For tumour accumulation experiments, micelles were injected at 100 μg per mouse on a platinum basis. Data are means ± s.e.m., $n = 6$. *$P > 0.05$; **$P < 0.05$; ***$P < 0.01$; ****$P < 0.001$.

Table S1), which are the major organs responsible for the clearance of nanocarriers[29]. The levels of accumulation of DACHPt/m in these organs are comparable to other polymeric micelles incorporating cisplatin[8] or doxorubicin[9], except for a slightly higher accumulation of 100 nm DACHPt/m in the liver. Because the surface chemistry and charge of nanocarriers have been reported to critically affect the interactions of nanocarriers with plasma proteins and cells and the biodistributions of nanocarriers[21,22,29,30], the analogous surface chemistry (PEG-coated surface), neutral charge and comparable plasma clearance of DACHPt/m with different diameters are substantial advantages for the evaluation of their extravasation, penetration and accumulation abilities in solid tumours as well as the associated therapeutic outcomes.

Antitumour activity of DACHPt/m in solid tumours

The antitumour activity and accumulation of DACHPt/m with different diameters were examined in tumour models with different permeabilities: a hyperpermeable murine colon adenocarcinoma 26 (C26) model characterized by high vascularization and slight tumour stroma[31] and a human pancreatic adenocarcinoma BxPC3 characterized by low vascularization, reduced vascular permeability due to pericyte coverage of blood vessels[20,31] and thick fibrosis, which are representative characteristics of some intractable solid tumours[20,31–33]. Note that the *in vitro* cytotoxicity of sub-100 nm DACHPt/m on C26 and BxPC3 cell lines was not substantially affected by micelle size (Supplementary Table S3), suggesting that their *in vivo* antitumour effect can be associated with their accumulation and microdistribution in solid tumours. In the C26 model, all micelles demonstrated comparable tumour growth inhibition (Fig. 2a), whereas oxaliplatin did not show a significant antitumour effect. The accumulation levels of all sub-100 nm micelles in C26 tumours were consistently comparable, reaching ~10% ID g^{-1} tumour at 24 h post-injection (Fig. 2b). In the BxPC3 model, the size effect of DACHPt/m on antitumour activity became evident, with the 30 nm micelles completely suppressing tumour growth, the 50 nm micelles leading to reduced antitumour activity, and the 70 nm and 100 nm micelles failing to show any antitumour effect (Fig. 2c). The accumulation of the 30 nm micelles was two times higher than that of the 50 nm micelles and four times higher than that of the 70 and 100 nm micelles after 24 h in BxPC3 tumours (Fig. 2d), which is also consistent with the antitumour efficacies in Fig. 2c.

The intratumoral microdistribution of fluorescently labelled DACHPt/m with different sizes in tumour sections was studied to investigate size-dependent extravasation and penetration of micellar nanomedicines in tumours. Histological investigations using haematoxilyn and eosin (H&E) staining revealed a well-vascularized medullary histological pattern of C26 tumours with reduced tumour stroma (Fig. 3a). In this tumour model, the fluorescence signals from the 30, 50, 70 and 100 nm micelles were uniformly distributed throughout the entire section at 24 h post-injection, suggesting deep tumour penetration of all sub-100 nm micelles (Fig. 3b, red). The immunofluorescence localization of platelet endothelial cell adhesion molecule-1 (PECAM-1), expressed by endothelial cells, indicated the extensive distribution of blood vessels in C26 tumours (Fig. 3b, green). However, H&E staining of BxPC3 tumours revealed the formation of nests of cancer cells surrounded by fibrotic tissue (Fig. 3c), which may act as a barrier

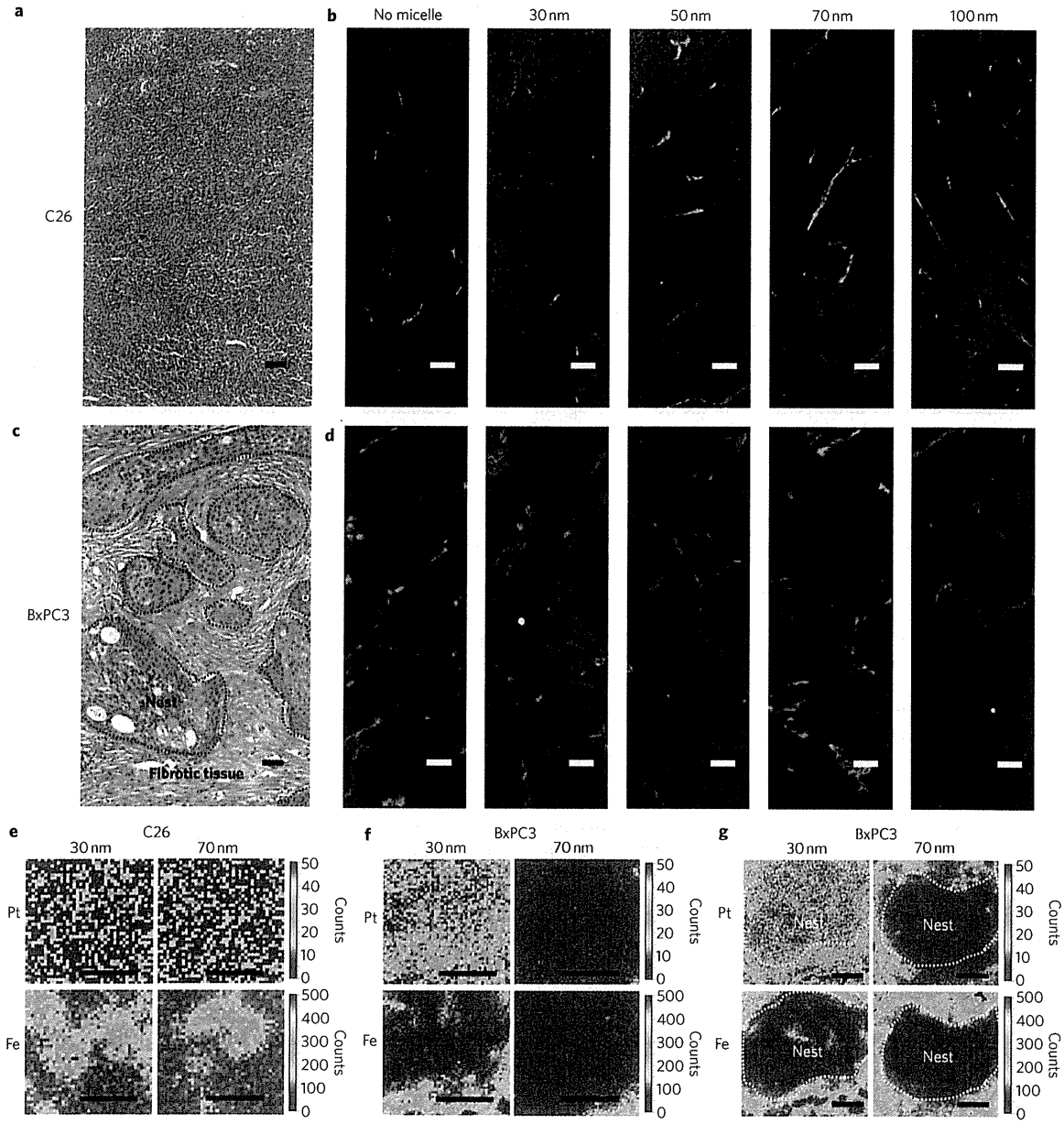

Figure 3 | Microdistribution of fluorescently labelled DACHPt/m of varying sizes in tumours. a–d, Histological examination of C26 tumour (**a**) and BxPC3 tumour (**c**) by H&E staining (dashed lines in **c** show area of cancer cell nests in the BxPC3 tumour) and fluorescent microscopic images of sections of C26 (**b**) and BxPC3 (**d**) tumours 24 h after intravenous administration of fluorescent micelles with different sizes. Micelles were labelled with Alexa 594 (red). Blood vessels were marked with PECAM-1 and Alexa 488 secondary antibody (green). Scale bars, 50 μm. **e–g**, Mapping of platinum atoms from DACHPt and iron from haemoproteins in tumour sections of C26 (**e**), BxPC3 (**f**) and a BxPC3 cancer cell nest (indicated by dashed line) (**g**) by μ-SR-XRF 24 h after administration of micelles. Scale bars, 50 μm.

against the penetration of drugs and nanocarriers[20,31]. In the BxPC3 model, immunofluorescence detection of PECAM-1 (Fig. 3d, green) indicated the presence of blood vessels around the cancer cell nests and the absence of vessels in the interior of these structures. We observed that the 30 nm micelles penetrated inside the tightly nested structures of BxPC3 tumours, but the fluorescent signal of the bigger micelles diminished and was concentrated close to the blood vessels, indicating their failure to enter the nests of cancer cells (Fig. 3d, red). This size-dependent penetration of fluorescent DACHPt/m may affect the intratumoral distribution of the delivered drug.

Given that the drug loaded in the micelles was a platinum complex, we assessed the drug microdistribution in tumour sections by detecting element disposition using μ-synchrotron radiation X-ray fluorescence (μ-SR-XRF). The very distinct peak of the platinum from the DACHPt can be observed in the sum spectrum of the line scan as well as the elements traditionally present in animal tissue. The distribution of iron and platinum in tumour tissue